

Defects in carbon nanotubes

4

Ali Ghavamian¹, Maksym Rybachuk^{1,2} and Andreas Öchsner³

¹Griffith University, School of Engineering, Engineering Drive, Southport, Queensland, Australia,

²Griffith University, Queensland Micro- and Nanotechnology Centre, Nathan, Queensland, Australia, ³Esslingen University of Applied Sciences, Faculty of Mechanical Engineering, Esslingen, Germany

4.1 Introduction

The modern world necessitates the development of new technologies and tools with better quality and efficiencies to quench the desire for time, cost, and energy saving. Among all aspects of this new tools design, the material selection is the critical step in designing man-made objects with enhanced functionalities and efficiencies. In this sense, nanomaterials offer novel, unique, and application-ready properties that can immediately meet and advance the areas as diverse as electronics and computing, composite materials construction and reinforcement, health and medicine, energy storage and conversion, defence and security, and other applied fields.

Since the discovery of carbon nanotubes (CNTs) in 1991 by Iijima [1], universal attention has been drawn to these carbon-based (C-based) nanomaterials owing to their advantageous and highly tuneable mechanical, electrical, and chemical properties and their application potentials in various nanoindustry fields [2].

4.1.1 Synthesis and production

There is a common trait between the CNT structure and the structure of a planar two-dimensional (2-D) graphene sheet. Both the CNTs and graphite are natural allotropes of carbon and both are composed entirely of sp^2 hybridized bonds with unhybridized π orbitals on each carbon atoms overlapping sideways and providing a massive $\pi-\pi^*$ system above and below the plane of the sheet of atoms. The CNTs, however are closed or open cylindrical nanostructures. Generally speaking, there are two types of CNTs, namely, the single-walled (SW-) carbon nanotube (SWCNT) type that are assumed to be created by rolling up a single graphene sheet into a single hollow cylinder and, the multi-walled (MW-) carbon nanotube (MWCNT) type, which is a result of one or several graphene sheets, rolling up into a set of concentric cylinders [3,4]. The industrial fabrication of CNTs, both the SW and the MW types, comprises of three basic steps that include the actual CNT synthesis, purification, and functionalization process. Different approaches have been historically used to synthesize CNTs including arc discharge, laser ablation, catalytic chemical vapor deposition (CVD) processes, flame synthesis, and silane solution methods [5] among a dozen others. In order to grow CNTs, typically, nanometer-size metal particles are required as

catalytic elements to convert carbon precursors into tubular carbon structures and to form encapsulating carbon overcoats. Most commonly used metal catalysts are Fe, Co, and Ni owing to their high carbon solubility at high temperatures and high carbon diffusion rate in these metals. However, non-metal catalysts such as nanodiamond particles [6], K₂CO₃ nanoparticles [7], and biomass [8] could also be applied among others for such a process [7].

Below, we briefly discuss the main processes known for quality CNT synthesis. The arc discharge method [9] is a high temperature process and was originally used by Iijima [1]. The process uses two graphite electrodes, placed in close proximity in an inert environment at low pressure. The discharge vaporizes an anode and small rod-shaped CNTs are formed on the cathode, see Fig. 4.1A [10,11].

During the laser ablation method [12–14], a piece of graphite is ablated using a nanosecond, picosecond laser above the target ablation threshold in an inert atmosphere. The CNTs are formed on a Cu substrate collector, which acts as a catalyst as illustrated in Fig. 4.2B.

The catalytic CVD process which is shown in Fig. 4.1C, uses a thermally activated volatile carbon-based precursor such as a hydrocarbon (i.e., methane, acetylene, etc.) or CO₂ gas which is introduced over a substrate that contains a catalyst, such as the earlier mentioned Ni, Co, or Fe nanosize particles which act as nucleation islands for the growing CNTs. Although the catalytic CVD process has been known since the late 1950s [15–18] the use of this process for C-based nanomaterials synthesis has only been taken up from the early 1990s. In addition, a variety of CNTs can be produced using the hydrocarbon flame synthesis where thermally activated hydrocarbon is mixed with metal aerosol catalysts. This approach is an effective way of using both the physicochemical and catalytic reactions for controlled growth of CNTs at relatively low (~1073 K) temperatures [19–21].

Another approach for producing CNTs is to immerse a substrate such as carbon paper or stainless steel mesh in a silane solution of a metal catalyst. Then by passing a carbon source gas such as ethylene through the heated substrate, the CNTs are produced on the conductive substrate as a result of the reaction between the catalyst and the passing gas [22].

Although a great variety of different methods have been developed for the synthesis of CNTs since the early 1990s, the catalytic CVD process as illustrated in Fig. 4.1 has remained a popular method as it is known to be more economical and versatile compared to both, the arc discharge and the laser ablation methods and can offer the production of CNTs of high purity and at (relatively) high yield. Both the SW- and MW-CNTs can be produced, using the catalytic CVD process and a reasonable control over the diameter of SW-CNTs. Although arc discharge is also an easy and not too expensive method for synthesis of both SW- and MWCNTs, the produced CNTs tend to be short with random sizes and directions and they often need purification. Finally, laser ablation technique can produce long CNTs with few defects. However, it is referred to as a costly approach for synthesis of CNTs, especially for MWCNTs' production as it requires an expensive laser and a high power requirement [23].

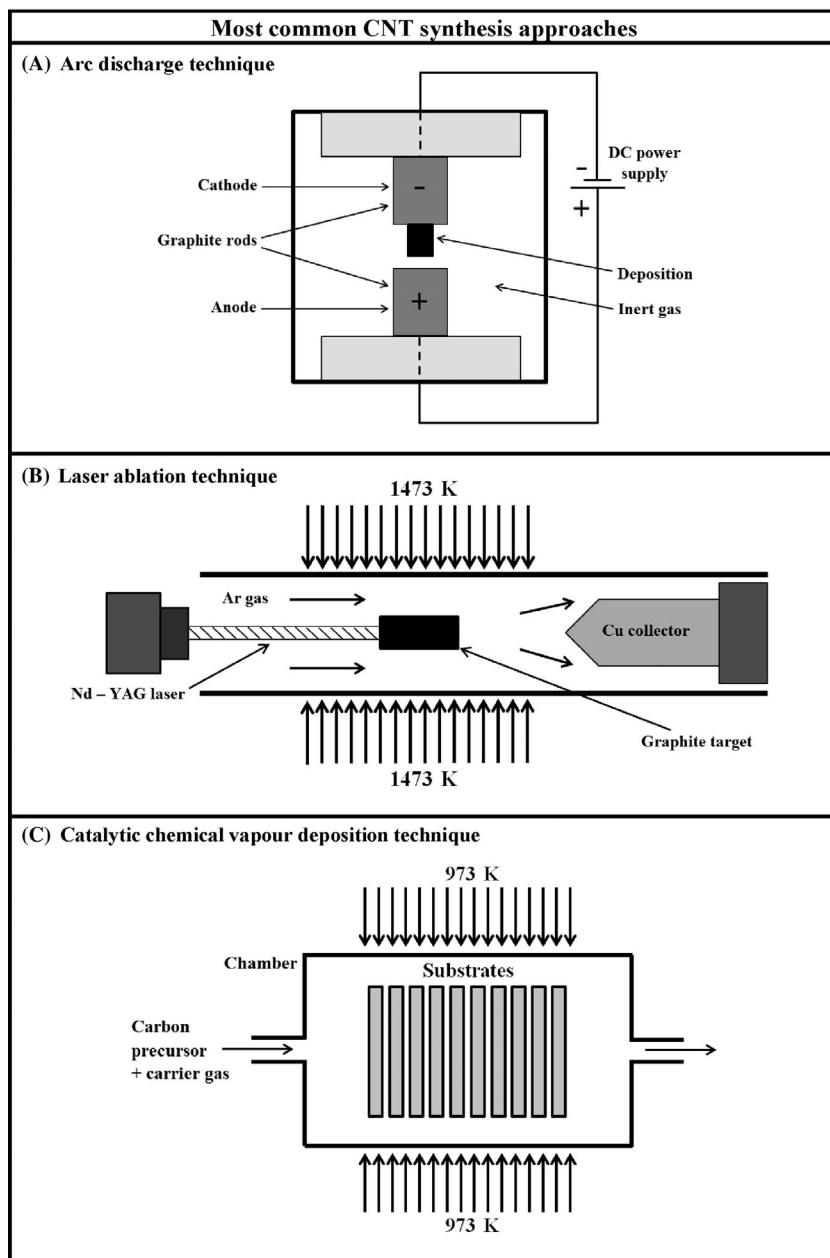


Figure 4.1 Schematics of most common CNT synthesis techniques: (A) arc discharge, (B) laser ablation, and (C) chemical vapor deposition techniques.

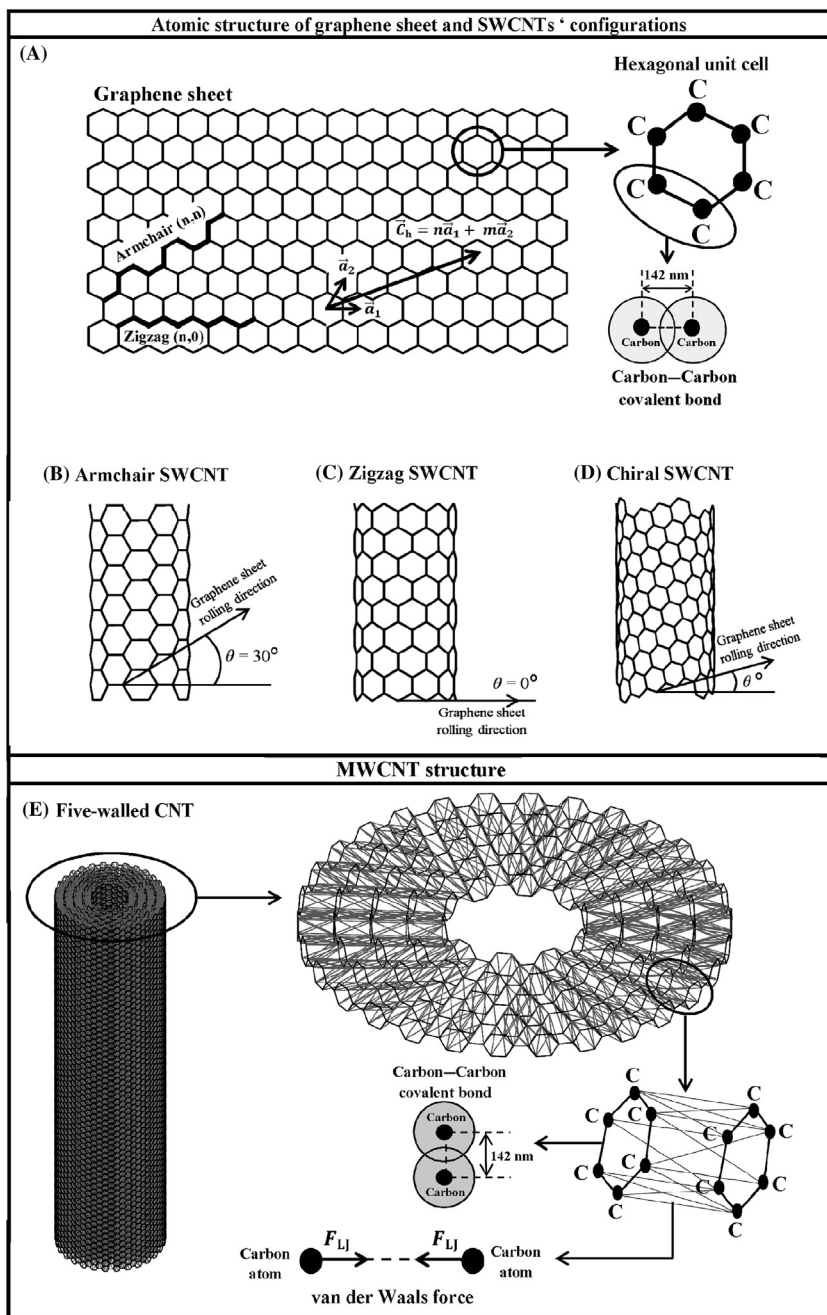


Figure 4.2 (A) Atomic structure of graphene sheet, (B)–(D) SWCNT configurations, and (E) MWCNT structure.

Source: Adapted from [75,149].

Following the synthesis process, the CNTs normally undergo a postprocessing treatment such as refinement and/or purification and, if needed, the functionalization as as-synthesized CNTs commonly contain considerable amounts of impurities such as inclusions of metal catalyst and metal oxide support materials, amorphous carbon (*a*-C) particles, and C-nanocrystallites among others. Notably, the purification stage can be discarded if the CNTs are produced of suitable quality and structural organization.

Generally, the purification of as-synthesized CNTs comprises of two steps that include a chemical treatment, followed by a mechanical impurity separation process. The former step is applied to make the impurities ready to be dislodged and physically removed from CNTs. Although both the SWCNTs and impurities are oxidized in this process, the structural damage to SWCNTs is negligible [5,24]. Acid cutting [25–27] using HCl is commonly employed to remove metal inclusion through solvation, followed by mechanical or gravimetric separation of solute species from CNTs. In the latter case, when, for example, a magnetic purification process is used, the CNTs are mixed with inorganic oxides nanoparticles, such as ZrO₂ or others, in an ultrasonic bath to mechanically remove the ferromagnetic catalytic particles from their graphitic shells and finally, to trap the particles with permanent magnetic poles. Following such chemical treatment, high purity CNTs, especially SWCNTs, are acquired [28]. In addition, the impurities can be mechanically removed from CNTs using sonication in a solvent. In this way, the impurities are forced to vibrate and consequently dispersed and mechanically segregated [5,29,30].

Other techniques are also commonly used to purify CNTs such as thermal annealing and microfiltration [31]. The annealing technique [32] is based on the fact that at temperatures in the range of 873–1873 K, C=C bonds undergo bond-reorganization that affects CNTs skeletal rearrangement; following the annealing process, selective bond cleavage is observed where structural defects are consumed through strain annihilation, whereas *sp*² graphitic carbon and low molecular weight fullerene nanoinclusions are pyrolyzed. In addition, the temperatures at or above 1873 K range is above the melting temperature for most metallic catalysts and therefore, heating CNTs to and above this temperature range allows the removal of most of the metal catalyst from the structure of CNTs. A relatively novel microfiltration CNT purification process [33] is based on selective separation of CNTs, based on their physical size and/or functional groups; this method allows to remove or seed-out common CNTs impurities such as metal catalysts, fullerenes, and carbon nanoparticles by means of physical filtering of impurities in a specially designed nanosized mesh or sieve.

Finally, functionalization or modification of CNTs is performed to introduce changes in the atomic structure of CNTs through controlled doping or structural reorganization in order to attain particular properties and functionalities for the desired applications. Generally, there are two types of covalent and non-covalent CNT functionalization [5]. Normally, covalent C-bonding with CNT sidewall surface is exploited by means of the chemical reactions of an adatom or dopant atoms

to bond with nanotube sidewalls in the process of covalent functionalization through selective oxidation and carboxyl-based coupling. Strong acids are also employed for creating the tube cap openings as well as the holes in the CNT sidewalls by an oxidation process [5,34]. Normally, for increasing the solubility of CNTs in aqueous solutions in such a modification process, the oxidation is introduced to the caps and sidewalls with the –COOH groups which also allows for covalent couplings with other molecules through amide and ester bonds. In addition, the process reduces van der Waals interactions between the tubes and enables the separation of CNT bundles into individual separated tubes. Regarding the fact that solubility of the CNTs has been a crucial argument, such a technique enables the CNTs to be conjugated with various functional groups and thus, bonding with appropriate groups serves the CNTs to become soluble in aqueous or organic solvents. An alternative approach for tuning the interfacial properties, increasing the solubility and preserving the structural properties of CNTs is non-covalent functionalization [5,35,36]. The corresponding dispersion procedures which usually involve ultrasonication, centrifugation, and filtration are commonly performed by surfactants, polymers, and biopolymers which provide quick, easy, cheap and efficient modification.

4.1.2 Applications

The exceptional properties of CNTs not only have drawn attention worldwide but have also opened a wide range of application potentials in nanoindustry as either stand-alone nanomaterials or reinforcement in composite materials. For example, CNTs can appear as considerably light materials with outstanding mechanical properties, such as high stiffness, strength, and aspect ratio, corresponding to which, the CNTs are highly welcome to be used as reinforcement in composite materials [37]. On the other hand, the advantageous electrical properties provide the opportunity of using CNTs as the next generation of semiconductors and nanowires in nanoelectronic components [38–40] and as electrodes in organic light-emitting diodes [41]. These nanostructures are also used as high-sensitivity microbalances [42], gas and molecule sensors [43], field emission type displays [44], tiny tweezers for nanoscale manipulation [45], probes in scanning probe microscopy and atomic force microscopy instrumentation [46] with the additional advantage of a chemically functionalized tip, as well as their application in hydrogen storage devices, due to their high surface-volume ratio [47]. Finally, a relatively low toxicity and nonimmunogenic behavior of functionalized CNTs highlights the potential of wide application of these nanomaterials for drug delivery applications as a new alternative and efficient tool for transporting and translocating therapeutic molecules. For such an application, the CNTs can be functionalized with bioactive peptides, proteins, nucleic acids, and drugs to deliver their cargos to cells and organs [48].

4.2 Defect-free CNT structures

4.2.1 Single-walled carbon nanotube

The similarity between the atomic structure of CNTs and graphene, enlightens the idea that an SWCNT can logically be imagined to be formed by rolling a graphene sheet into a carbon-built hollow cylinder or a tube [49]. It is known that the wall thickness of an SWCNT has been assumed many times to be equal to the diameter of a single carbon atom (0.34 nm) [49,50], whereas the outer diameter of SWCNT is normally within the range of 1 to 50 nm and the overall length can often exceed 10 μm [50]. Similar to graphene sheets, CNTs' atomic structures are constructed of honeycomb-like hexagonal unit cells, each of which is constructed of six carbon atoms. Each of these carbon atoms is bonded to three neighboring carbon atoms by covalent C–C bonds with a bond length of 0.142 nm [49], as illustrated in Fig. 4.2A.

Generally, a CNT is distinguished by its configuration which is normally defined by its chirality, or helicity that is expressed by its corresponding chiral vector \vec{C}_h , expressed by Eq. (4.1), in terms of two unit vectors \vec{a}_1 and \vec{a}_2 and two integers m and n (steps along the unit vectors), or the chiral or twisting angle θ by which the graphene sheet is assumed to be rolled into an SWCNT [49], see Fig. 4.2A.

$$\vec{C}_h = \vec{n}a_1 + \vec{m}a_2. \quad (4.1)$$

Based on the CNTs chiral vector or chiral angle, there are three fundamental CNT configurations, i.e., armchair, zigzag, and chiral as shown in Figs. 4.2B–D. In terms of the chiral vector (m and n) or in terms of the chiral angle θ , if $m = n$ or $\theta = 30^\circ$, an armchair CNT is created. Likewise, a zigzag CNT is formed when $\theta = 0^\circ$ or $m = 0$, and finally, a chiral structure is constructed when $0^\circ < \theta < 30^\circ$ or $m \neq n \neq 0$. The radius of an SWCNT is also calculated by Eq. (4.2) where $a_0 = \sqrt{3}b$ and $b = 0.142$ nm is the C–C bond length [49],

$$R_{\text{CNT}} = \frac{a_0\sqrt{m^2 + mn + n^2}}{2\pi}. \quad (4.2)$$

4.2.2 Multi-walled carbon nanotube

MWCNTs are formed when two or more concentric SWCNTs form a single structure. Therefore, the atomic structure of MWCNTs and SWCNTs are identical. However, for MWCNTs, weak nano-covalent van der Waals interactions between the adjoining planar wall surfaces (i.e., planar graphene sheets) should also be taken into consideration. The van der Waals forces act between every two carbon atoms on the two neighboring walls in the structure of MWCNTs and are defined using the Lennard–Jones potential relation as [49]:

$$F_{\text{LJ}} = \frac{dV_{\text{LJ}}}{dr} = \frac{4\epsilon}{r} \left[-12\left(\frac{\sigma}{r}\right)^{12} + 6\left(\frac{\sigma}{r}\right)^6 \right], \quad (4.3)$$

where r is the distance between two carbon atoms and $\sigma = 0.3851\text{nm}$ and $\epsilon = 0.4396\text{kJ} \cdot \text{mol}^{-1} = 0.072997284 \times 10^{-20}\text{J}$, are referred to as the Lennard–Jones parameters which are material-specific. Although the Lennard–Jones force is generally considered a weak force, it is strongly repulsive when the two atoms are close to each other and it is mildly attractive when the inter-atomic distances are large [49]. Fig. 4.1E shows the atomic structure of MWCNTs and the corresponding covalent bonds and van der Waals forces acting between carbon atoms.

4.3 Defects and disorder in CNTs

According to the experimental observations, the structure of CNTs is often disordered and commonly contains a number of defects [23]. Defects in CNTs are normally present as an intrinsic artefact owing to a specific CNT synthesis or postfabrication processing for a given application.

4.3.1 Macroscopic defects in CNTs

Macroscopic or large-scale defects in CNTs are defined as defects that change the straight principle axis of defect-free CNTs into a curvature or coil-shaped line or cause irregularity in the hexagonal unit cell in the CNT structure which reduces the structural homogeneity of the CNT and alters their properties. For instance, the initial curvature presents a curved principle axis for the curved CNTs (see Fig. 4.3A) [3,51] as well as the structural twisting which results in irregularity in the CNTs' hexagonal unit cells and changes these cells from the regular to a slant form [52].

Kinks or angular bends in the structure of hetero-junction CNTs are another macroscopic defect types which are created when two SWCNTs of different chirality are joined to form a single CNT with a hetero-junction structure. Apart from the kink in the structure of hetero-junction CNTs, these CNT types could appear straight or bent, based on the configuration of the connecting tubes. Straight hetero-junction CNTs are created when the connecting CNTs are of the same configuration, while the bent hetero-junction CNTs are a result of the connection between the CNTs with different configurations, as illustrated in Fig. 4.3C [53]. A similar defect and connection can also happen when three or more CNTs are merged covalently to form a molecular junction or multi-terminal junction CNTs with various geometries of X, Y, and T shapes [54]. Fig. 4.3D shows different molecular junction CNTs.

Finally, the spiral defect which deforms the CNTs from their original perfect straight shape occurs when the tube is twisted like a spring, along its longitudinal axis which creates a completely new version of CNT with different properties [55].

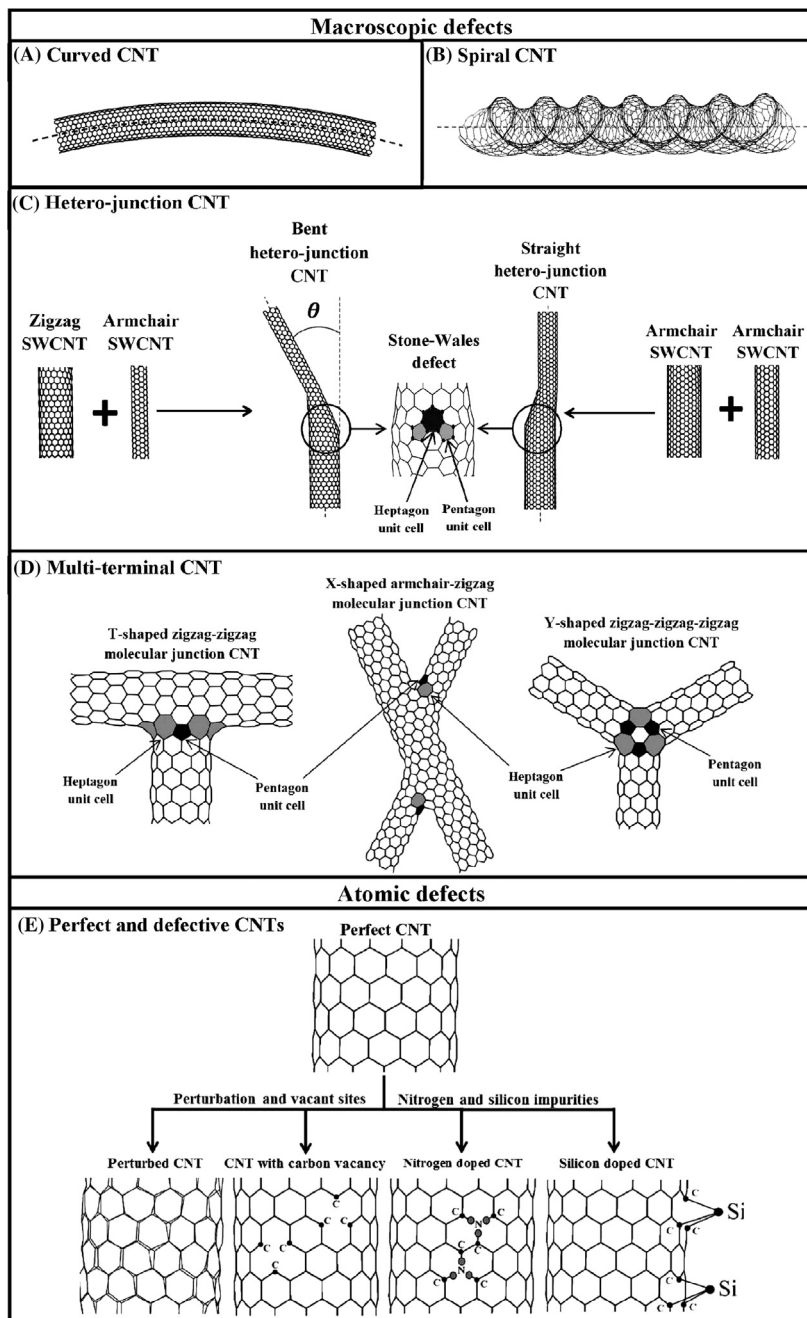


Figure 4.3 Macroscopic (large scale) and atomic defects in the CNTs.
Source: Adapted from [2,62,210].

Based on this spiral angle which is illustrated in Fig. 4.3B, several CNTs can be created with different configuration.

4.3.2 Atomic scale defects in CNTs

The atomic scale defects in CNTs, such as atom vacancies, adatoms, dopants, and/or impurity inclusions, cell perturbations (polygonization) (see Fig. 4.3E), and Stone–Wales defects (Fig. 4.3C), are generated during the CNTs synthesis or post-processing processes in order to intentionally alter and tailor the structure of “as-fabricated” CNTs for specific applications. Atom vacancies and doping are created when a finite number of carbon atoms in CNT structure is removed or replaced with carefully selected dopant atoms (commonly Si, B, N, P, etc.) creating Schottky and/or Frenkel defects, respectively [56–59]. Depending on the degree of the lattice mismatch between the neighboring carbon atoms and the dopant elements, the dopant species can emerge from the CNT structure, resulting in a high degree of structural inhomogeneity and bond disorder in CNTs. Perturbation or polygonization occurs when all of the carbon atoms in the structure of CNTs are dislocated in the 3D space for random fractions of the C–C bond length, which changes the circle shape of the cross-sectional area of CNTs into polygon shapes and causes the CNT to completely lose its homogeneity [60].

The Stone–Wales defect happens when two or more CNTs are joined to construct a hetero-junction or multi-terminal junction CNTs. These connections are possible only when the required pentagon–heptagon cell pairs are inserted to replace some hexagonal unit cells in the connection places. Such an atomic defect which creates a kink (a heptagon–pentagon knee) and in some cases, an additional bending in the structure of hetero-junction and molecular junction CNTs removes the homogeneity in both large and atomic scale and alters the properties of these CNT types [61,62].

4.3.3 Tailoring CNTs properties by means of defect introduction

Although both macroscopic and atomic scale defects reduce the homogeneity of CNTs and significantly alter their properties, mainly the mechanical properties, the addition of adatoms into the CNT structure is an effective way to tailor physico-chemical properties of the tubes for specific applications such as field emission devices, *n*–*p*-type nanojunctions, electrical connectors, photo-optical sensors, and others. Doping of CNTs can considerably improve the chemical reactivity of CNTs which paves the way for their unique applications as miniature gas detector elements, effective catalytic materials, protein immobilizers, and others [38,39,62–64].

Boron, nitrogen, and phosphorus have been conventionally used as the *p*- (B) or *n*- (N, P) dopants that provide a relatively straightforward and technologically achievable means for tailoring electronic properties of CNTs through substitutional doping [65].

In this regard, the N-doped CNTs, especially the N-doped MWCNTs, have been found as ideal active electronic components in applications for high-response rate

gas sensors and field- and electron-emission tips, as nitrogen offers high chemical reactivity to the pure inert CNTs as well as providing metallic behavior which allows N-doped CNTs to be applied as composites fillers with considerable electrical conductivity, combined with outstanding mechanical strength of the CNTs [65–67]. Likewise, phosphorus which is an *n*-dopant shows considerable chemical reactivity and improves charge carrier mobility and density of CNTs by acting as scattering centers as well as strongly modifying the chemical properties of the surface of CNTs by demonstrating chemical reactivity and sensing capabilities which enables the P-doped CNTs to be employed as ultrasensitive molecular sensors and as a support for the cathode catalyst in fuel cells, with a higher electrocatalytic activity and lower cost, compared to the currently used platinum catalysts [68,69].

As the incorporation of boron in the structure of CNTs enhances their electrical conductivity and capacitance, the B-CNTs have also been successfully employed as active electronic components in common consumer products such as capacitors and electron storage batteries [70,71]. A quick comparison between the *p*- and *n*-dopants reveals that despite high doping efficiency, the electrical properties of N- and P-doped CNTs can be easily affected by an O₂ absorption from the device operational environment, whereas B-doped CNTs are generally more robust owing to decreased electronegativity and, subsequently, the oxidation potential of B-doped CNTs systems and therefore, they are less affected by environmental conditions [72].

Recently, Si-doped CNTs have been developed specifically for nanodevices, designed to operate at high temperatures, high power, and in harsh environments. Silicon atoms are inserted into the CNT molecular structure as a substitutional impurity and given the lattice mismatch between the Si-guest and C-host structure, the heavily-doped Si-CNTs display significantly higher chemical reactivity, compared to the undoped or B-, N-, or P-doped CNTs. So far, the Si-doped CNTs have been considered for applications in ultrafast electronic nanodevices and chemical adsorbents [73,74].

While doping is a widely-recognized conventional mechanism for functionalization of the CNT structure and properties, an instance of structural modification of the CNT structures is to join two CNTs about their axis of symmetry by means of hetero-junction connections using molecular construction. Such hybrid CNTs are expected to inherit the CNT properties, i.e., high mechanical flexibility, stiffness and lightness as well as high electrical conductivity which has made them widely applicable as solar cells with considerable efficiencies. The metallic and semiconducting nature of these CNTs also awards them a potential to be used as all-carbon building blocks in mechanical and electronic nanodevice systems [75–78]. Similarly, molecular junctions are constructed by connecting two or more CNTs which could be used as multi-terminal electronic devices [54].

As each of these defects and modifications has its own disadvantages and shortcomings, based on the application and the required properties, a certain combination of these modifications could compensate for those shortcomings to some extent or sum up the advantages of the corresponding modifications to produce more efficient CNT-based nanodevices. For example, Si-doping in the structure of hetero-junction CNT solar cells leads to higher air stability, better power-conversion efficiencies,

negligible degradation of current density after hundreds of hours of exposure to air, and easier manufacturing and lower production costs [79,80]. Another example can be the incorporation of boron in nitride CNTs which not only can tune the conducting properties of CNTs but also increases the environmental resistance of N-doped CNTs by controlling the concentration of substitutional N atoms in the carbon lattice and the N-doped CNTs oxidization [81].

4.4 Characterization and findings

4.4.1 Characterization approaches

The characterization of CNTs is an important step that cohesively joins together efforts, aimed at selecting suitable fabrication methods for production of CNTs with predetermined properties and determining appropriate new applications of these unique nanostructures. Despite the increasingly large number of available analytical techniques, none can be considered as the most popular, universal, and widespread today. These techniques employ a variety or a combination of probing media, such as electrons or photons, ions and neutral atoms, protons and neutrons, and acoustic waves to probe the structure and properties of CNTs. The signal and/or secondary effects, collected from CNTs can be monitored as functions of at least one variable including the signal intensity magnitude, relative and absolute energy values, respective time and relative angle of recoil, absolute and relative phase composition, mass (i.e., atomic, molecular), and temperature. Given the large number of probing media to secondary signal data combination, below we summarize the most widely used characterization techniques for the study of CNT structural ordering and organization.

The characterization approaches are generally divided into two groups of experimental and theoretical methods. The most common experimental analysis approaches are microscopy and spectroscopy analytical methods that use photons (including X-rays) and electrons as means to directly probe the atomic and molecular composition, including degree of atomic and structural disorder, and physicochemical properties of CNTs.

Microscopy techniques that provide pseudovisual information about the structure and properties of CNTs include scanning electron microscopy (SEM), scanning probe- and tunneling microscopy (SPM/STM), transmission electronic microscopy (TEM), and atomic force microscopy (AFM). By means of using SEM it is possible to obtain detailed information on the morphological details of CNTs structure as well as differentiate between different CNTs and other nanomaterials of similar structure and size. Considerable details of CNT structures, namely the number of carbon layers in their walls can be obtained by means of a high-resolution TEM. Details about the surface and/or core functionalization of tubes can also be characterized using both the SEM and TEM. Conventional, low-resolution SEM is able to reveal the presence of individual CNTs on the surface and inside the core matrix of composite materials employing the charge-based subsurface imaging modes

[82,83]. The use of TEM allows the probing of inter-shell spacing of CNTs, based on Lambert's law. The observation of freestanding, detached, and isolated CNTs is not common as often, the CNTs are adjoined together in hexagonal close-packed arrays, held together by the van der Waals forces and thus, the application of TEM, coupled with electron diffraction technique allows the investigation of complex CNTs structures [84–90].

The detailed atomic structure of CNTs can also be observed and investigated using the STM and SPM measurements. The STM images provide the 3D morphology of tubes and resolved images of both, the atomic structure and the electronic density of states (DOS). Based on the fact that the electronic properties of CNTs are dominated by their chiralities and diameters, the chiral angle of CNTs can be effectively measured by STM to investigate and predict the observed CNTs properties [91–96]. Apart from the STM/SPM measurements, the AFM is the most widely used approach for characterization of CNTs structure providing the direct and accurate 3D reconstruction of the sample topography with atomic resolution within a short time with almost no limitation on the sample size to be analyzed. The AFM approach is based on measuring the interaction forces between the AFM cantilever tip and the sample allowing precise and accurate measurements of CNTs structure, morphology and CNT interactions with a variety of supporting substrates and probing media [97–100].

Complimentary to microscopy measurements, the near edge and X-ray absorption fine structure spectroscopy (NEXAFS/XAFS), soft X-ray absorption spectroscopy (SXAS), X-ray reflectivity and diffraction (XRR/XRD) spectroscopy, X-ray photoluminescence and Auger spectroscopy (XPS/Auger), general photoluminescence (PL), near and infrared (N-IR/IR) and Raman spectroscopy are commonly employed for detailed studies of the atomic structure, composition, and bonding disorder of CNTs. The NEXAFS/XAFS, SXAS are comprehensive approaches, normally accessible at national synchrotron facilities, that allow direct and precise measurements of CNTs electronic structure, atomic composition, structural disorder, including determination of the degree of bond hybridization in mixed sp^2/sp^3 -bonded carbon materials [101]. The NEXAFS/XAFS measurements are based on the analysis of electron excitations from the C1s and valence bands to partially filled and empty states. The relative peak positions, peak intensities, and spectral line shapes in NEXAFS/XAFS spectrum are directly related to the nature of the unoccupied electronic states in CNTs as the electron yield spectrum is created as a result of the emission of Auger electrons from valence molecular orbitals which is caused by decay of core hole states. The decay of core holes may also take place through the emission of fluorescent photons, originating from the top 200 nm of the film as opposed to Auger electrons, which arise from the top 10 nm, expressing the fact that this technique is both, surface and bulk sensitive and also both, the CNT electronic structure and surface functional groups can be investigated simultaneously. Moreover, in carbon-based materials such as CNTs, this technique not only can measure and detect specific bonds in molecules but also the angular dependence of the specific involved orbitals can also be revealed. Also, the presence of functionalized species and chemical impurities can be determined by

NEXAFS/XAFS and SXAS as well as the intramolecular bond length, and the location and intensity of the lower-energy $\pi-\pi^*$ resonance, which allow precise determination between the sp^2 and the sp^3 hybridized bonding in complex structure of CNTs [101–103].

For multi-layer CNT systems, less sophisticated measurement approaches such as the XRR measurements are used, by which the layer by layer properties of multi-layer CNT structures, such as the layer roughness, thickness, and density distributions can be determined. The XRR measurements provide a fast and sensitive approach to determine the individual layer thickness and inter-diffusion crystallization state of the multi-layer CNT samples as well as individual CNT layer density and nano and microroughness values; the samples for XRR measurements, normally, do not require any particular preparation or treatment [104].

Similar to the XRR measurements, the XRD provides information on the inter-layer spacing, structural strain, impurities, and curvature in the structure of CNTs as well as relative CNT alignment. As the CNTs are randomly organized relative to the X-ray incident beam, the statistical characterization of CNTs, performed by XRD, allows precise monitoring of CNT diameters and chiralities distributions, as well as detection of a number of layers in MWNTs. Unlike the NEXAFS/XAFS or SXAS, the XRD is not well suited for differentiating the microstructural details between the CNTs and the graphite or graphene structures. However, the sample purity (i.e., the presence of catalyst, functional groups) can be successfully determined by the SRD method [105,106].

CNTs whose chemical structure and elemental composition has been modified by means of the synthesis or production process or due to the chemical interaction with organic compounds or adsorption of gases are commonly investigated using the XPS method. The XPS spectra are obtained by irradiating a sample with a beam of X-rays while simultaneously measuring the kinetic energy and number of electrons that escape from the uppermost (less than 10 nm deep) layer of the material being analyzed. The use of XPS requires high vacuum or ultrahigh vacuum conditions, although a current area of development is ambient-pressure XPS, in which samples are analyzed at pressures of a few tens of millibar. In application to CNTs, the XPS is used to measure the elemental composition, obtain the relative weight (wt. %) and atomic (at. %) composition of elemental impurities in the samples (i.e., N, P, B, Cr, Ni, Fe, etc.), analyze the electronic state of each element, based on their respecting binding energy levels and as certain the uniformity of elemental composition across the uppermost surface (by means of line profiling or mapping), or uniformity of elemental composition as a function of ion beam etching (i.e., depth profiling) [107–109].

The PL measurements are based on bulk characterization of CNTs, and allow differentiation between the semiconducting CNT, based on their band gap energy levels that relate to their chirality and is also inversely correlated to CNT diameters. The PL phenomenon is based on that fact that van Hove singularities are observed in the DOS of CNTs governed by $\pi-\pi^*$ bonds. The optical emission of the semiconducting tubes is caused by main transition, called E_{11} and the sharp inter-bands transitions (E_{22} and ...) between the corresponding van Hove singularities in the

valence and conductance bands. The PL emission only occurs with E_{11} transition while a wide range of wave length (from N-IR to UV) is useful for the PL excitation. As the energy of the van Hove singularities maxima mainly depends on the CNTs' diameter, various superpositions of distinct E_{xx} transitions appear with different wave lengths for different SWCNTs and thus, the CNTs' characteristics can be extracted as well as the presence of chemical defects and the purity of the samples [110–117].

The N-IR and IRIR spectroscopy is commonly used to characterize CNTs and to determine CNT size (i.e., diameter, length, orientation), based on IR active modes and/or regions. For example, SWCNTs display nine IRIR active symmetry-dependent modes that include the chiral, zigzag, and armchair CNT orientations, among these, the two main A_{2u} and E_{1u} modes are different between different CNTs. Using the N-IR and IR measurements of the size of CNTs, the degree of impurity inclusions which have remained from the synthesis or imposed to the CNT for the modification of their structures can also be determined [118–123].

One of the most efficient, fast and non-sample destructive techniques for characterization of carbon nanotubes is Raman spectroscopy. Normally, Raman is used to observe vibrational, rotational, and other low-frequency modes in CNTs and carbon-based systems. This approach is based on the Raman effect, which is the inelastic scattering of photons after their interaction with vibrating molecules of a given material. During this inelastic interaction, photons either transfer energy to (Stokes- Raman) or receive energy from (anti-Stokes Raman) molecular vibrations, or phonons, giving the energy change of the scattered photons equal to the vibrational energy levels of the molecules in the sample. Since vibrational energy spectrum depends on the chemical composition and molecular ordering of the sample (i.e. elemental composition, bond strength, bond angle disorder, lattice symmetry, etc.), a Raman spectrum is sample specific and provides excellent mean for evaluation of chemical composition and structural ordering and organisation of CNTs [124–126].

For characterization of SWCNTs and DWCNTs (double-walled CNTs) by this technique, different features which are sensitive to the chiral indices (n,m) and chiral vector, are presented by Raman spectra. These features are the radial breathing mode (RBM) where all the carbon atoms are moving in-phase in the radial direction, the G-band where neighboring atoms are moving in opposite directions along the surface of the tube as in 2-D graphite, the dispersive disorder induced D-band, and its second-order related harmonic G'-band. Among these four features, the RBM demonstrated more sensitivity to the nanotube diameter (d_t) [127], as expressed in Eq. (4.4).

$$\omega_{\text{RBM}} = \frac{A}{d_t} + B, \quad (4.4)$$

where ω is the vibration frequency, and A and B are constants. However, in some of the previous research, only the constant A has been used in determination of the CNT diameter [128–132].

Based on this approach, the SWCNTs can be characterized, based on different bands. The diameter distribution of the nanotubes in a particular SWCNT bundle can be obtained by measuring RBM for many laser energies as these transition energies (E_{ii}) is unique for each chirality set (m,n) and enlightens the fact that the G-band is an intrinsic CNT feature that closely corresponds to the vibrations in all sp^2 carbon materials and demonstrates the difference between the material types and reveals whether the nanotube is semiconducting or metallic by showing the lower and higher frequency components, associated with vibrations along the circumferential direction and vibrations along the G direction of the nanotube axis. The D- and G'-bands, which depend on chirality and diameter of nanotubes, correspond to the defects in the structure of CNTs. The D-band in graphite generally involves scattering of defects, i.e., porous, impurities, or other symmetry-breaking defects in sp^2 carbons in the graphene sheet, while the second-order G'-band is observed for defect-free sp^2 carbons [130–133].

In characterization of MWCNTs by Raman spectroscopy, most of the characteristic differences that distinguish the Raman spectra in SWCNT from the spectra for graphite are not so evident in MWCNT. This limitation comes as a result of large outer tube diameters of typical MWCNTs as they are constructed of concentric SWCNTs with diameters from small to very large ones. For instance, with a good resonance condition established, the RBM Raman feature, corresponding to a small diameter inner tube, can sometimes appear. However, it does not usually occur as the RBM signal from large diameter tubes is usually too weak to be observable and the ensemble average of inner tube diameter broadens the signal. Due to the effect of the diameter distribution within the individual MWCNT, and also the variation between different tubes in an ensemble of MWCNT in typical experimental samples, the G-band in MWCNT is small in intensity and smeared out and, consequently, the G-band feature predominantly demonstrates a weakly asymmetric characteristic line shape, with a peak appearing close to the graphite frequency. Only in the case of the electron irradiation of MWCNT could the most effective influence of radiation be anticipated. The obtained feature can be explained by a possible appearance of radiation defects which seem to be created by broken bonds, appearing during creation of vacancies and contributes to the degradation of the nanotubes [124–126].

It is also advantageous to mention that in Raman spectroscopy, the sample preparation is not necessary and all the allotropic forms of CNT i.e. fullerenes, carbon nanotubes, amorphous carbon, polycrystalline carbon etc. are active. However, the quantitative determination of each type is impossible at present [134,135].

Although the experimental techniques provide invaluable information about the structural and atomic properties of CNTs, many properties of CNTs, particularly, many mechanical properties and their long-term behavior in many particular circumstances and conditions are very costly, difficult, and sometimes impossible to be determined and predicted, due to the nanoscale sizes of these nanomaterials and the limitations in the required experimental tools and technology. Therefore, theoretical and computational approaches, employing the density functional theory (DFT), continuum mechanics (CM), molecular dynamics (MD), and finite element

method (FEM) have been developed and proposed to simulate, characterize and predict the behavior of CNTs and carbon-based nanostructures.

The DFT is a computational approach, based on the quantum mechanical theory, used in physics, chemistry, and materials science to investigate the electronic structure (principally the ground state) of many-body systems, in particular, atoms, molecules, and the condensed phases. Using the DFT method, the properties of a many-electron system, such as CNTs, can be determined by using functionals (i.e., functions of another function), which in this case, is the spatially dependent electron density. The DFT approach chemically characterizes the nanomaterials, based on the Schrödinger wave equation for all relevant electrons of the system, in which the positions and element identity of all atoms, describing the nanostructure is required as input of such an equation. The DFT is popular in computational physics and chemistry calculations because of its capability of calculation in solid-state physics and quantum chemistry, low costs, and higher accuracy, compared with other similar traditional approaches. However, the DFT is limited to a finite number of atoms and precise description of inter-molecular interactions, accurate estimation of van der Waals forces, and estimation of the degree of dopant interactions for complex systems [136–140].

One of the simplest ways for theoretical modeling of CNTs is the application of continuum mechanics for the simulation of the mechanical behavior of CNTs, modeled as a continuous 2D or 3D structure. Based on the CM approach, the CNTs are considered as a continuum pipe and thus, can be simulated as an isotropic shell model with particular length, diameter and thickness, and elastic properties (i.e., Young's modulus and Poisson's ratio). The modeling is based on the assumption of linear and elastic behavior of CNTs which can provide an accurate description of the system at small strain. However, CNTs can demonstrate nonlinear behavior in their displacement-strain diagram. Likewise, as the section ratio t/R is not small, the beam model also becomes more efficient for long SWCNTs and therefore, the basic deformation modes such as tension/compression, bending, torsion, buckling, and vibration results could be readily obtained from beam theory. Although the shell model can be easily implemented into numerical codes or classical mechanics analytical calculations to be used for mechanical characterization of CNTs, the disadvantages of this approach emanates from the fact that in such a modeling the atomic characteristics have been neglected. For example, the chirality of CNTs is only expressed by the radii of the CNTs which is not sufficient in many cases. In addition, the force among the atoms and also the atomic defects cannot be simulated by such a modeling technique [141,142].

The MD approach is commonly employed to investigate the motion of atoms and determines the instantaneous location and velocity of each atom in the materials structure, using the Newtonian dynamics function in order to perform the force analysis and energy calculation for obtaining the atom distribution at different thermodynamic states for structural characterization. Generally, the MD simulation works based on the calculation of Hamilton dynamics equation for every atom, which is a function of location, momentum, time, and also kinetic energy and

potentials of atoms where the coordinates and momentum (velocity) of atoms are the initial values and conditions, respectively, in the equilibrium state. This MD approach comprises of four stages of determination of initial location and velocity of atoms, evaluation of equilibrium state, the loop for adding new atoms and evaluation, and analysis and calculations. In the MD approach some function such as the Brenner function is employed for simulation of bonding among atoms to correctly reflect the construction and destruction of the interactions among the atoms. Meanwhile, many types of force field functions such as the Lennard–Jones function whose parameters can be obtained from experimental data for C₆₀ or graphite can be employed for the definition of the molecular interactions among the different CNTs [143–146].

The FEM, also known as the finite element analysis (FEA), is a popular numerical method for solving problems of engineering and mathematical physics. This approach, which generally requires the solution of partial differential equations in boundary value problems, builds a system of algebraic equations for which the values of the unknowns at discrete number of points over the determined domain are numerically calculated and approximated. For such an approximation, the model is divided into a finite number of parts, called elements. Then by solving the problem for these elements, the problem for the whole system, which has been subdivided into smaller and simpler problems for these elements, will be solved by recombining the simple equations, corresponding to the model elements into a larger system of equations that describes the entire model [147]. Generally, two typical FEM models of CNTs can be presented.

The first and simplest FE modeling is based on the CM, based on which the CNTs are assumed to be a continuum isotropic pipe or shell, simulated in a finite element software with defined geometric properties, namely, length, diameter and thickness, and material properties, e.g., Young's modulus, Poisson's ratio, etc. Then, by subdividing the model to a finite number of elements, the corresponding mesh is created and finally characterized by simulating mechanical tests under defined boundary conditions [148].

The second and more accurate mechanical characterization of CNTs by FEM/FEA is based on the CNTs' honeycomb structures, in which each CNT is assumed to be a cylinder-shaped truss with nanoscale dimensions, constructed of the links with nanoscale lengths which represent covalent C–C bonds. For a typical finite element modeling and characterization of CNTs, normally a hexagonal unit cell is created in a finite element package (e.g., the commercial codes MSC.Marc or ANSYS) by employing six nodes which represent individual carbon atoms, connected by beam elements. Then, such a unit cell is copied around the CNT's longitudinal axis to form a single ring and, finally, this single ring is copied along the principle axis of the CNT to construct a SWCNT structure. Finally, materials and geometric properties of the beam elements, which are calculated by a linkage between solid mechanics and molecular mechanics concepts, based on the energy approach, using the quantities, called force field constants (K_r , K_θ , and K_φ) as shown in [Table 4.1](#), are introduced to the model elements which represent C–C bonds to complete the CNT simulation. The simulation of MWCNTs almost follows

Table 4.1 Material and geometric properties of a C–C covalent bond

Material and geometric properties of carbon–carbon covalent bond				
Force field constants	E (Young's) modulus = $\frac{k_r^2 b}{4\pi k_\theta}$	R_b (bond radius) = $2\sqrt{\frac{k_\theta}{k_r}}$	$I_{xx} = I_{yy}$ (second moments of area) = $\frac{\pi R_b^4}{4}$	A_{c-c} (cross-section area) = πR_b^2
$k_r = 651.97 \text{ nN/nm}$, $k_\theta = 0.87 \text{ nN. nm/rad}^2$, $k_\varphi = 0.27 \text{ nN.nm/rad}^2$	$5.48 \times 10^{-6} \text{ N/nm}^2$	0.0733 nm	$2.2661 \times 10^{-5} \text{ nm}^4$	0.0169 nm 2

Source: Obtained from [75].

the same steps by creating two or more concentric SWCNTs. However, there is an additional step that is the definition of van der Waals forces between the CNT walls. With regards to the fact that such a force is dominated by the distance between every two atoms and is independent of mass, the van der Waals force can easily be simulated by a spring with no mass and calculated by Eq. (4.5), based on the Lennard–Jones potential relation where r is the distance between two carbon atoms, Δr is the change in their distance due to CNT deformation and the stiffness $k = 0.24245 \text{ N/m}$. Eventually, by setting up the desired boundary conditions, namely arbitrary displacement or twist, the reaction force or torque will be calculated by the solver and displayed as an output of the FE package which could be used to determine some properties of CNT, e.g., Young's and shear modulus or critical buckling load by classical mechanics relations. However, some of the mechanical properties such as vibration modes of CNTs can be obtained directly as an output of the commercial package too [149,150].

$$F_{vdW} = \frac{4\epsilon}{r} \left[-12 \left(\frac{\sigma}{r} \right)^{12} + 6 \left(\frac{\sigma}{r} \right)^6 \right] + k\Delta r. \quad (4.5)$$

4.4.2 Experimental findings

Since the discovery of CNTs, numerous experiments have been performed for the characterization of these nanomaterials and consideration of the influence of different defect and functionalization types which have led to new and beneficial properties for these novel materials.

An experimental study was performed by Lu [151] for the evaluation of the tensile and shears moduli of CNTs, considering the empirical force constant. Based on his results, high Young's modulus of 0.97- and 1 TPa were obtained for SWCNTs

and MWCNTs, respectively, as well as a general value of 0.5 TPa for the shear modulus of CNTs.

Salvetat et al. [152] also used an experimental investigation for mechanical characterization, particularly Young's modulus of CNT, based on TEM and AFM. Their results showed that Young's moduli for MWNTs are as high as those for graphite and even higher for small SWCNTs. They also reported that the disorder in the structure of CNTs leads to lower elastic modulus. However, quantifying such disorders seemed to be difficult by experimental methods.

Song and Youn [153] characterized the CNT reinforced nanocomposites and probed the influence of the CNT dispersion on their properties. For such an experiment, they synthesized CNTs by CVD technique and used epoxy resin as the matrix of the corresponding composite. The results from FESEM (field emission scanning electron microscopy) and TEM revealed that the poorly dispersed CNTs/epoxy composites have a more solid-like behavior, including higher storage modulus, less elastic modulus, and complex viscosity, compared with the ones with well dispersed CNTs. Moreover, the incorporation of CNTs led to an increase in the strength and conductivity of the composite. Moreover, the thermal and electrical conductivity of well dispersed CNT composites appeared to be higher than the poorly dispersed one.

Shanmugharaj et al. [154] employed acid treatment, followed by a reaction with multifunctional silane, 3-aminopropyltriethoxysilane for performing the surface functionalization of MWCNTs as well as investigating the influence of silane-functionalized CNTs on the rheometric and mechanical properties of natural rubber composites by FT-IR, EDX (energy dispersive X-ray analysis), and Raman spectroscopy. This demonstrated an enhancement in the rheometric properties of the reinforced polymers, such as scorch time and optimum cure time, as well as an increase in their modulus and tensile strength as a result of better interaction between the CNTs and NR vulcanizates.

Zhu et al. [155] used an optimized $H_2SO_4/70\% HNO_3$ acid treatment and subsequent fluorination of SWCNTs for enhancing their dispersion in an epoxy composite by dissolving the functionalized SWNTs in dimethylformamide and mixing the resultant sample with the epoxy resin which led to highly dispersed and well integrated SWCNTs in the epoxy composite with an increase of 30% and 18% in the modulus and the tensile strength of nanocomposite, respectively, due to the improvement in the SWCNTs dispersion in the composite.

Paiva et al. [156] performed a mechanical characterization of polymer–carbon nanocomposites under torsion. For such a characterization, they functionalized the CNTs with poly (vinyl alcohol) (PVA) and then, produced the nanocomposite films with homogeneous nanotube dispersion by embedding the water-soluble PVA–functionalized CNTs into the polymer matrix. The results demonstrated significant improvement in the mechanical strength of the functionalized CNT-reinforced nanocomposite, due to better CNT dispersion in the matrix and more efficient interfacial bonding between the CNTs and the hosting polymer matrix.

Mitchell et al. [157] employed in situ generation for producing polystyrene nanocomposites with functionalized SWCNTs and evaluated the functionalization

influence on the CNTs dispersion in polystyrene. Their results showed better dispersion of the functionalized SWNCT in the nanocomposite as well as an improvement in the compatibility between the SWCNTs and the polymer matrix, compared with the unfunctionalized CNT-reinforced nanocomposites.

Dai et al. [158] probed the conductivity of individual nanomaterials, based on their structures by conventional lithography to electrically contact single ends of nanomaterials, as well as a force microscope, equipped with a conducting probe tip for simultaneous mapping of the structure and resistance of the portion of the material protruding from the macroscopic contact. Their results with respect to CNTs revealed that the structural defects such as curvature and also pentagon–heptagon defect led to substantially higher electrical resistivity of CNTs.

Xie et al. [159] synthesized aligned and isolated CNTs with high density, high purity, and uniform diameters via CVD technique and characterized the mechanical and physical properties. Based on their results, it was proved that the CNTs produced by CVD are not defect free and involve defects as their thermal conductivity and electrical conductivity are about two orders of magnitude lower than those of defect-free crystalline graphite at room temperature. It was also understood that the defects in the structure of CNTs led to lower tensile strength and Young's modulus.

Ruoff and Lorents [160] researched the mechanical and thermal properties of CNTs, compared to graphite properties. They reported that unlike graphite, the thermal expansion of CNTs appears to be isotropic. However, the thermal conductivity may be considerably anisotropic and high along the long axis, compared with other materials. They also pointed out that for producing high-strength composites, SWCNTs with an open end would be a better choice, compared with MWCNTs. It was also discussed that although the appropriately pretreated and modified SWCNTs may react well with the matrix to form a strong continuous interface in the structure of the composite, the defects and modifications could substantially change the properties of SWCNT fibers.

Sun et al. [161] synthesized lipophilic and hydrophilic dendra for functionalization of CNTs and improving their solvability via amidation and esterification reactions. The electron microscopy and optical spectroscopic techniques and TEM images revealed that the functionalized CNTs are soluble in common organic solvents, such as hexane and chloroform, and water to form colored homogeneous solutions to be applied for trapping of metal nanoparticles in solution.

Zeng et al. [162] developed Poly (ϵ -caprolactone)-functionalized CNTs by covalently grafting and coating poly (ϵ -caprolactone) (PCL) onto the surfaces of MWCNTs which resulted in core/shell structures with nanotubes as the hard core and the hairy polymer layer as the soft shell. Their characterization from FTIR, NMR, SEM, TEM, and Raman spectroscopy demonstrated good solubility and dispersibility of the MWNT–PCL nanohybrids in low-boiling-point organic solvents.

Kong et al. [163] developed Pd-functionalized CNTs and investigated their properties of acting as molecular hydrogen sensors by electron-beam evaporation of Pd over the entire substrate containing the SWNT. The AFM images revealed high sensitivity, fast response, and reversibility of Pd-functionalized CNTs sensors toward hydrogen molecules at room temperature.

Sanip et al. [164] also studied the influence of functionalized CNTs on the gas separation properties of mixed matrix membrane. For such an investigation, they embedded functionalized CNTs into the polyimide membrane and the resultant membrane was characterized for the separation of CO₂/CH₄ gases. Based on their results, an improvement of 100% was observed in the gas separation properties of the resultant membranes, compared with the corresponding neat polymer membrane.

Chen et al. [165] developed an experiment to study the protein and other biological molecules immobilization potential of non-covalent functionalized SWCNTs, synthesized by directly suspending them on meshed gold grids via the CDV process. Based on their TEM and AFM images, the protein molecules were observed densely on the SWCNT bundles while they appeared with gaps between them on the individual SWCNTs. They also concluded that such an approach could also be extended for many other systems, namely inorganic nanoparticles.

An experimental investigation was performed on the CNT potentials for drug design and discovery by Prato et al. [166]. Based on their report, the functionalization potential and the reactivity of CNTs as well as their ability to be conjugated with different functional groups serve to carry simultaneously several moieties as well as their ability to contain many molecules, ions, or metals in their internal space, which supports the application potential for pharmaceuticals design with targeting, diagnosis, and drug and gene transport purposes. However, the toxicity argument and the level of biocompatibility of CNTs is a crucial discussion for their biomedical applications.

Singh et al. [167] also researched the capability of ammonium- and lysine-functionalized CNTs for the transport of biologically active molecules and DNA delivery for vaccination and the construction of a CNT-based gene delivery system. The functionalized CNTs demonstrated different degrees of DNA condensation efficiencies which seemed to be dominated by the nanotube surface area and charge density. Moreover, large surface area showed considerably high DNA condensation efficiency, while not appearing to be necessary for effective gene transfer.

Hu et al. [168] characterized chemically functionalized CNTs by a systematic study for their application as substrates for neuronal growth. Their results revealed that not only the biocompatibility, durability, and inertness of CNTs serves to apply them in implants where long-term molecular cues for neurite outgrowth is necessary for cell regeneration after spinal cord or brain injury, but also the chemical modification of their tips and chaining their surface could provide the chance to guide and control the neurite outgrowth and branching to avoid the transient retention of attached molecules to the CNTs.

Charlier et al. [169] investigated the structural and electronic properties of pentagon–heptagon pair defects in CNTs, using tight-binding models. It was understood that these defects not only change the tube diameter and chirality, but also dominate the electronic behavior around the Fermi level. The resonant states were also observed in the DOS, as a result of different peculiar sites in the five- and seven-membered rings. They also mentioned that where the defects are aligned along the cylindrical axis of the tube, the topological structure is more stable after tight-

binding MD relaxation, compared with the geometries with defects distributed along the circumference of the tube.

4.4.3 Theoretical investigations

Apart from experimental characterization of CNTs and the CNT-based nanomaterials, recently the theoretical and computational approaches and particularly computer-aided simulations have extensively been employed for the characterization of these nanomaterials, especially for their mechanical and physical properties, in their defect-free and defective forms to avoid the experimental characterization costs, difficulties, and limitations and to save the time and energy.

One of the common theoretical approaches for investigation of the atomic structures and properties of CNTs is DFT which has popularly been used by scholars. Sánchez-Portal et al. [170] performed *ab initio* calculations, based on the pseudopotential-DFT to probe mechanical properties of different SWCNTs. According to their results, the Young's moduli of CNTs which did not demonstrate a systematic dependency to the radius or the chirality were obtained to be very close to the one for graphite. Such a similarity was also observed between the Poisson's ratio of CNTs and graphite which appeared to be chirality dependent, except for a possible slight reduction for the CNTs with small radii. The sensitivity of the high-frequency optic modes of CNTs to their chirality and radius was also observed as well as their tendency to diminish with decreasing radii by effect of the curvature.

Ma et al. [171] investigated the behavior of vacancies in a graphene sheet and SWCNTs, using spin-polarized DFT. For such an investigation, they employed the periodic plane wave VASP code for their calculation and implemented the generalized gradient approximation of Perdew. According to their results, the vacancies in the structure of graphene had magnetic behavior and the symmetry of the sheet was broken by the distortion of an atom next to the vacancy site. In the SWCNT case, the vacancies demonstrated the capability of changing the electronic structure of SWNTs and converting some metallic nanotubes to semiconductors and vice versa. They also reported that ferro- or ferrimagnetism is observed in metallic nanotubes while some of the semiconducting nanotubes with vacancies showed an antiferromagnetic order. They concluded that the magnetic properties of vacancies are dominated by the chirality of the tube as well as the configuration and concentration of vacancies.

Mirzaei and Gulseren [172] employed the DFT to study the stabilities and properties of CNT-functionalized uracil–acetate hybrids structures. For such a research, they optimized CNT–UAH, CNT–UAM, and CNT–UA-hybrids to reach their minimum energies. Then, they obtained the values of total energies directly by DFT calculations as the overall nuclear and electronic energies. Based on their results, among these hybrids, the CNT–UAM and UAM appeared to be more stable. It was also observed that the existence of functionalized CNTs could modulate the orbital energy levels of the CNT–UA hybrids.

Kinoshita et al. [173] employed first principle DFT calculations to evaluate the mechanical properties of SWCNTs with 1D IMJs as well as the influence of pentagon and heptagon defects at the junctions on the mechanical and failure strength of IMJs. Their results indicated an increase in the strength and elongation of CNT–IMJs which appear as a result of the deformation concentration on a seven-membered ring. They also specified that the position of pentagon and heptagon pairs dominates the tensile strength and breaking strain of CNT–IMJs. However, the numbers of pentagon and heptagon pairs do not significantly influence CNT–IMJs properties.

El-barbary et al. [174] used DFT to investigate the behavior of monovacancy and B-doped defects in carbon hetero-junctions. According to their results, the highest surface reactivity was observed for the B-doped zigzag–armchair hetero-junction. The carbon atom removal was found to be easier from the network of hetero-junction armchair–armchair CNTs, compared with the zigzag–armchair and zigzag–zigzag hetero-junctions.

With respect to the long and complicated numerical operations in the theoretical characterization of defect-free and defective CNTs and, on the other hand, the capability of computers for performing fast and accurate solving operations for the intricate problems, recently computer-aided simulations have been proposed and broadly employed on the basis of the theoretical methods, i.e., CM, MD, and FEM by many scholars. In the following, a summary of computer-based research works on the mechanical properties of defect-free CNTs is provided in [Table 4.2](#) and subsequently, a literature review on numerical characterization of defective CNTs and the influence of different defects and modifications will be presented.

Che et al. [194] used empirical bond order-dependent force field and MD simulation to study the effect of structural defects and vacancies on the thermal conductivity of CNTs. Their results demonstrated that vacancies and conformational defects (5, 7, 7, 5) in the structure of CNTs appeared to decrease their thermal conductivities. However, such a decrease from the conformational defects was milder than vacancies as these defects do not change the basic bonding characteristic and causes much less overall structural deformation than vacancies.

Sammalkorpi et al. [195] developed a MD and CM simulation to investigate the mechanical properties of CNTs and the influence of vacancies. According to their results, the concentrated vacancies in the structure of CNTs caused a decrease in their tensile strength to 60%. The decrease of 50% was also observed in the critical strain of the tubes. Unlike the tensile strength and critical strain, Young's modulus of CNTs was not considerably affected by vacancy concentration. It was also observed that the vacancy damage can be healed by saturating the dangling bonds and, therefore, the vacancy-caused decrease in the mechanical strength of the CNTs can be alleviated. They finally proposed an expression for calculation of the Young's modulus of defective CNTs at an arbitrary, but not very high vacancy concentration [196]. Likewise, the atomistic structural mechanics investigation by Georganzinos et al. revealed a noticeable reduction in the natural frequency of SWCNTs as a result of the vacancy defect.

Table 4.2 Literature on the mechanical properties of defect-free and homogeneous CNTs

Evaluation of the mechanical properties of homogeneous CNTs, based on different approaches		
Researcher	Methodology	Obtained results [Young's modulus (E), Shear modulus (G) and critical buckling load (P_{cr}) and natural frequency (f)]
Yakobson et al. [175]	Continuum mechanics	The mechanical properties of CNTs are strongly dependent on helicity and atomic structure of the tubes. The influence of the curvature and chirality on the mechanical behavior of CNTs cannot be captured in an isotropic shell model, due to neglecting the discrete nature of the CNT geometry in this method.
Ru [176]	Continuum mechanics	The van der Waals (vdW) forces between the walls of CNTs are not noticeably dominant on the critical strain for the infinitesimal buckling load of a DWCNT.
Silvestre et al. [148,177]	Continuum mechanics	Shallow shell theories are not accurate for CNT analysis, due to CNT non-shallow structure. Some parameters, such as wall thickness of CNTs are not well defined in the CM.
Hu et al. [178] Chen and Cao [141]	CM Molecular dynamics and CM	$220 \text{ GHz} < f < 1450 \text{ GHz}$ for SWCNTs Three models of SWCNTs, i.e., space frame, shell and beam models were generated and their thermal vibrations were studied. The continuum models are more efficient to evaluate the overall deformation of SWCNTs at much larger length- and time-scales than pure MD analysis.
Lu et al. [179]	Molecular dynamic	Aspect ratios of SWCNTs and MWCNTs are inversely correlated to their critical buckling loads and the size of the outermost shell dominates the buckling behavior of MWCNTs.
Liew et al. [180]	Molecular dynamic	An optimum diameter for buckling load peaks of SWCNTs was obtained.
Li and Chou [181]	Molecular dynamic	Young's modulus of SWCNTs varies with the change in their diameters and chiralities. An increase in the diameter of the CNTs leads to monotonically higher elastic modulus and a closer Young's modulus to the one for grapheme sheet.

(Continued)

Table 4.2 (Continued)

Evaluation of the mechanical properties of homogeneous CNTs, based on different approaches		
Researcher	Methodology	Obtained results [Young's modulus (E), Shear modulus (G) and critical buckling load (P_{cr}) and natural frequency (f)]
Wang et al. [182]	Molecular mechanics	The buckling behavior of SWCNTs upon axial compression is dependent on the chirality of CNTs.
Chang et al. [183]	Molecular mechanics	Zigzag tubes have more buckling resistance than armchair models with the same diameters and the influence of the van der Waals interaction between the layers of DWCNTs is rather negligible.
Hu et al. [184]	Molecular structural mechanics and FEM	The buckling behavior of carbon nanotubes with large aspect ratios can be predicted by Euler's beam buckling theory while, for the models with small aspect ratios, the buckling behavior resembles the ones for thin-walled shells.
Kalamkarov et al. [185]	Continuum mechanics-based FEM and analysis	E and G for SWCNTs were obtained equal to 1.71 and 0.32 TPa, respectively from analytical calculations. $0.9 < E < 1.05$ TPa and $0.14 < G < 0.47$ TPa from FEM results.
Avila and Lacerda [186]	Finite element method	E was reported between 0.97 and 1.30 TPa for CNTs.
Nahas and Abd-Rabou [187]	Finite element method	E was obtained 1.03 TPa for CNTs.
To [188]	Finite element method	E and G for SWCNTs were obtained 1.024 and 0.47 TPa, respectively.
Rahmandoust and Öchsner [189]	Finite element method	For MWCNTs, 1.32 and 1.58 TPa for E and the range of 0.37 to 0.47 TPa for G were obtained.
Yao et al. [190]	Finite element method	Bending deformation and their buckling behavior of SWCNTs and MWCNTs were evaluated. An explicit relationship between the critical bending buckling curvature and the diameter, length and chirality of the CNTs was derived.
Fan et al. [191]	Finite element method	For MWCNTs, $E = 1$ TPa and $G = 0.35$ and 0.45 TPa. Aspect ratios of DWCNTs are inversely correlated to their critical buckling loads.

(Continued)

Table 4.2 (Continued)

Evaluation of the mechanical properties of homogeneous CNTs, based on different approaches		
Researcher	Methodology	Obtained results [Young's modulus (E), Shear modulus (G) and critical buckling load (P_{cr}) and natural frequency (f)]
Rahmandoust and Öchsner [192]	Finite element method	The buckling vulnerability of SWCNTs was confirmed. High accuracy of classical Euler equation for CNTs critical buckling load calculation was confirmed by FEM results.
Mir and Hosseini [193]	Finite element method	Natural frequency (f) of SWCNTs of different lengths, obtained: 0.0122 GHz $< f <$ 0.0448 GHz for zigzag SWCNTs, 0.0145 GHz $< f <$ 0.0764 GHz for armchair SWCNTs.

An MD simulation of CNTs was developed by Garg and Sinnott [197] to investigate the influence of the chemical functionalization on the mechanical properties of CNTs under compressive load. A comparison between the functionalized and unfunctionalized CNTs showed that the maximum buckling force decreases by 15% as a result of covalent chemical attachments, regardless of the CNT's chirality or radius.

Buckling behavior of both defect-free and defective SWCNTs was probed by Xin and Han [198] via MD simulation. The buckling strength of SWCNTs seemed to be dominated by the length, chirality, temperature, and the initial structural defects of the tubes. The existence of carbon vacancies was eventually observed to decrease the buckling strength of CNTs.

The influence of waviness, vacancies, aspect ratio, and length on the vibrational behavior of SWCNTs was investigated by Amjadipour et al. [199], based on MD simulation. Their investigations showed that an increase in the waviness and vacancy ratios decreased the natural frequency. Furthermore, the decrease in the length of SWCNT was reported to cause a reduction in its critical waviness ratio which indicates that in shorter SWCNTs, waviness has a more dominant effect on the natural frequency, compared to vacancies.

Finite element simulation of defective CNTs with curvature, spiral shape, twisting angle, z-distortion along the longitudinal axis, and xy-distortion along the radial axis was also proposed by Imani Yengejeh et al. [200–205] and their tensile, torsion, and buckling behavior was investigated. Their results clearly showed that the curvature in the CNT structures leads to lower tensile, torsion, and buckling strength. Likewise, the spiral distortion was observed to reduce the structural stiffness and Young's modulus of these nanomaterials. Finally, twisting and any

distortion was also found to decrease the CNTs tensile, torsion, and vibrational stabilities.

Lu and Bhattacharya [206] probed the influence of randomly occurring Stone–Wales defects on mechanical properties of CNTs by an atomic simulation. Their results showed that fracture occurs invariably in the defect location, while in the defect-free tubes, the crack initiates at quite random locations. Linear deformation was observed at halfway of the force–displacement curve. However, a clear yield point could not be determined. The increase in the number of such defects also led to a general decrease in the mechanical strength and ultimate strain of CNTs. However, no particular trend was observed for such a decrease.

The influence of the arrangement and distribution of defects (Stone–Wales defects and carbon vacancy) on the natural frequency of CNTs was explored by Shariati et al. [207]. They observed that these defects cause a reduction in the fundamental frequency of the tubes. However, the vacancy defect appeared to influence the vibrational properties of CNTs significantly more than the Stone–Wales defect.

Imani Yengejeh et al. developed a FE simulation of straight hetero-junction CNTs and investigated their mechanical properties. Their results showed that the existence of Stone–Wales defects in the junctions of nanotubes leads to a decrease in their Young's modulus, when compared with the values of their corresponding initial homogeneous CNTs. Their torsion, buckling, and vibration test simulation indicated that the twisting angle, the critical buckling load, and natural frequency of straight hetero-junction CNTs lie within the value ranges of those of their fundamental tubes [37,208–210]. Furthermore, their study on atomically defective hetero-junction CNTs with perturbation, dopings, and vacancies revealed that the atomic defects considerably decrease the tensile, torsional, and buckling strengths of the CNTs [211,212].

Mechanical properties of the CNTs with intramolecular junctions (IMJs) was investigated by Qin et al. [213] via MD simulation. Their results showed that the rupture strength of a junction is close to that of its thinner CNT segment, and the rupture strain and the Young's modulus significantly depends on its geometry. The damage and rupture of MWCNTs junctions was also predicted to emerge in the innermost layer and then propagate consecutively to the other layers.

Liu et al. [214] studied the deformation behavior of X-junctions by a MD simulation which showed that the breakage location depends on the junction strength. Based on which, if the junction is strong, the original bonding structures around the junctions remain safe and the bonds break at individual nanotubes, rather than at the junction region. However, for some (3,3)–(3,3) junctions and X-junctions formed by (5,0)–(5,0) tubes, the reconstruction of bonds at the junction region break took place which caused the transformation of a 3D junction into a 2D type.

Buckling behavior of IMJs was studied via MD and FE simulation by Kang et al. [215]. Based on their results, the critical compressive strain did not show sensitivity to the strain rate of relatively low range. However, it was observed that such a strain is significantly dominated by the strain rate under high speed

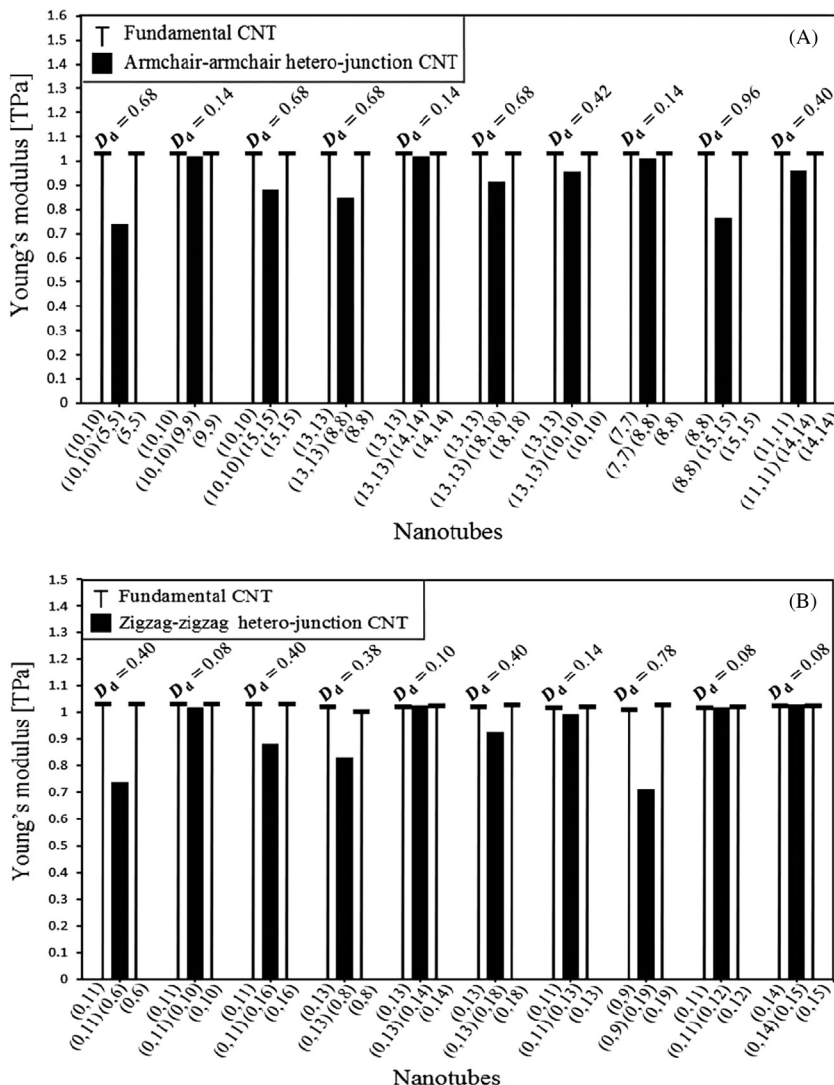


Figure 4.4 (A)–(F) Young's modulus of hetero-junction and homogeneous CNTs.
Source: Adapted from [219].

compression. Critical compressive strain of the IMJs also demonstrated dependency on their length and radial dimensions but was insensitive to their chirality.

The tensile strength of boron nitride CNTs (BN-CNTs) and the influence of point, line, and Stone–Wales defects on the CNTs properties was evaluated by Sarma et al. [216] via MD simulation. The Young's modulus of (10,0) BN-CNTs

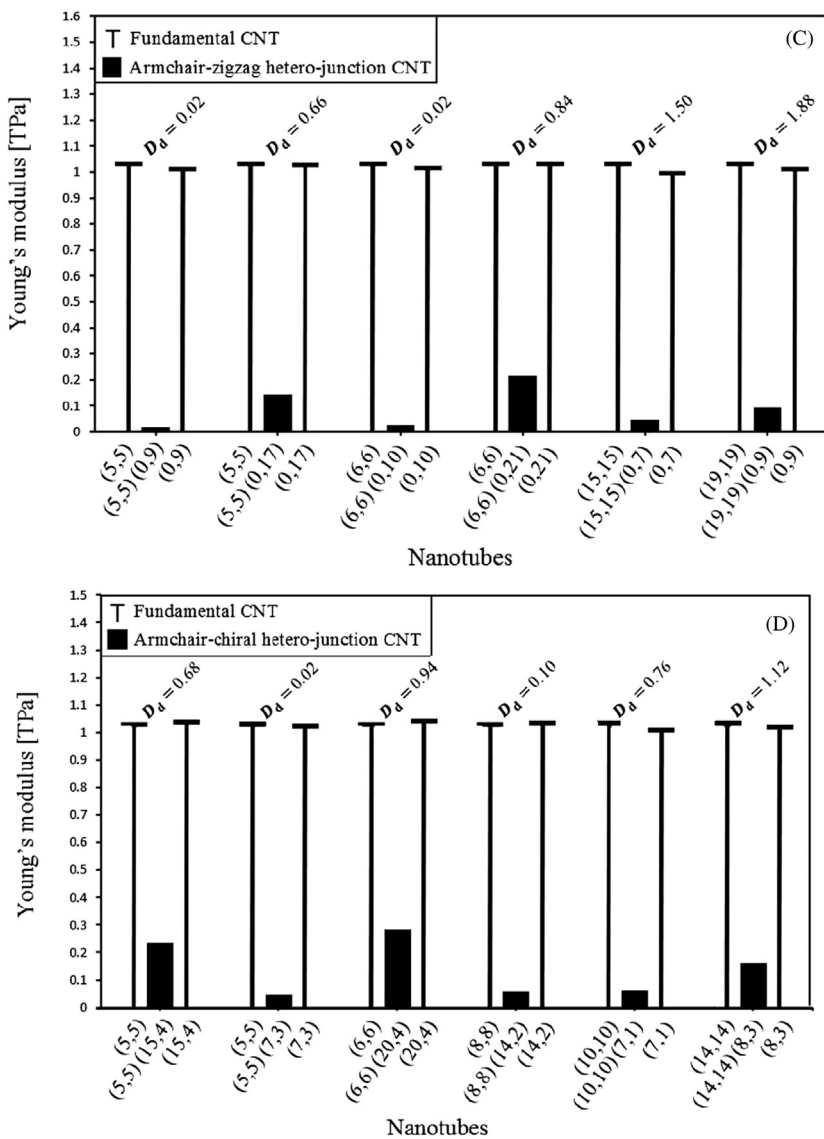
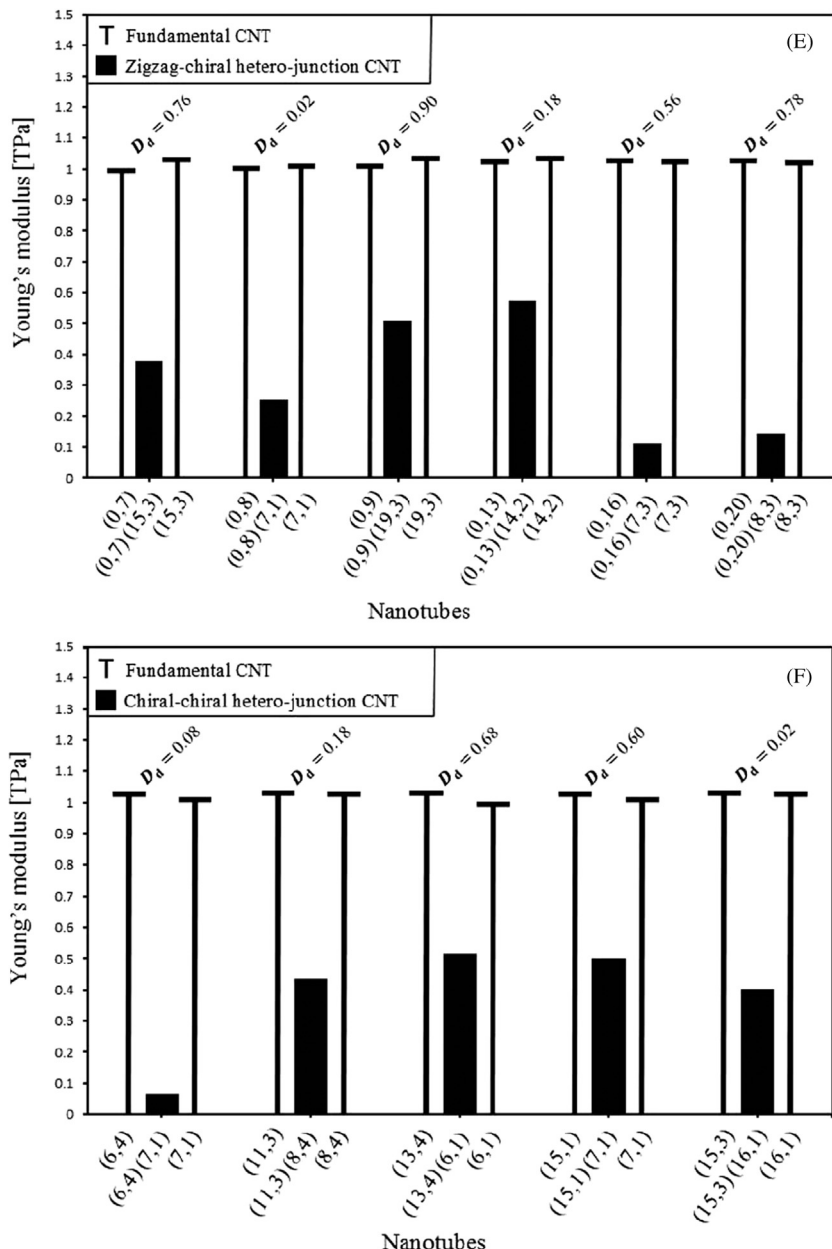


Figure 4.4 (Continued).

was about 1.098 TPa. It was also observed that the tensile strength of the tube was considerably reduced as a result of these impurities.

The elastic properties of BN-SWCNTs were explored by Jiang and Guo [217] via an analytical study, based on a molecular mechanics model. They finally proposed closed-formed expressions for Young's modulus, Poisson's ratio, and surface

**Figure 4.4** (Continued).

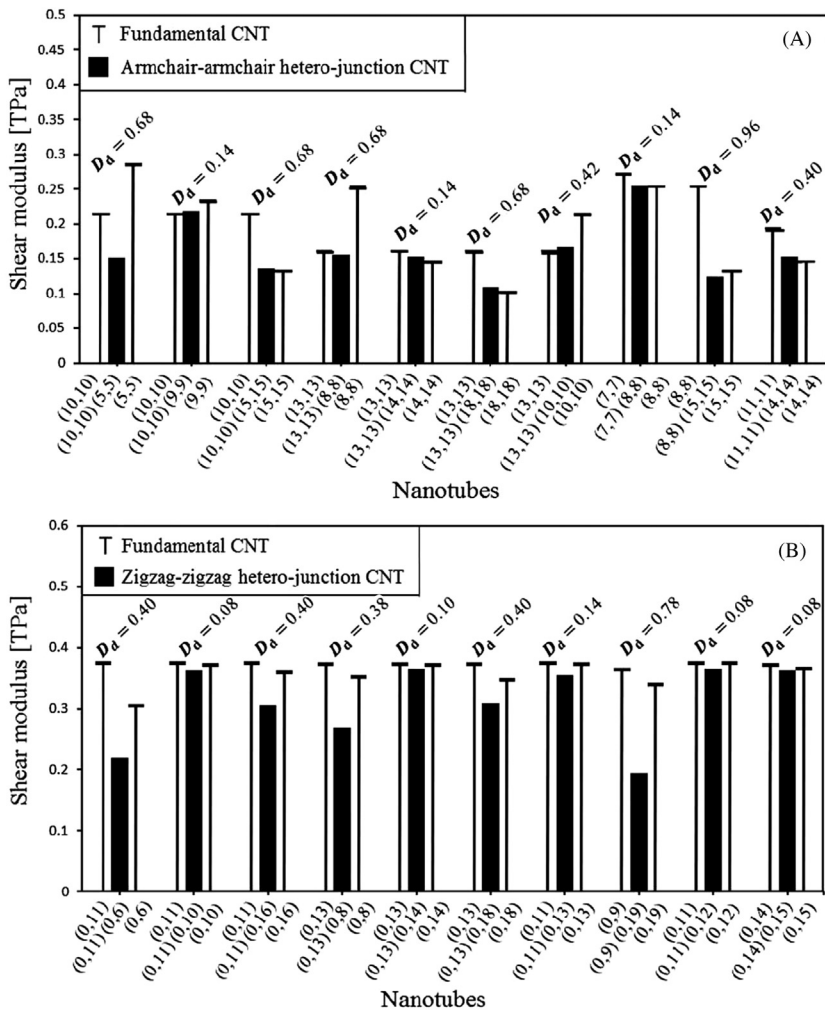


Figure 4.5 (A)–(F) Shear modulus of hetero-junction and homogeneous CNTs.

Source: Adapted from [219].

shear modulus as functions of the nanotube diameter. It was also perceived that their findings appeared to be helix angle sensitive and comparable to those from *ab initio* calculations.

Rahmandoust and Öchsner [218] evaluated the effect of the atomic defects, i.e., perturbation, vacancies, and Si-doping, on Young's modulus of the atomically defective SWCNTs which finally led to the fact that the elastic stiffness of SWCNTs faces a considerable decrease as a result of such defects.

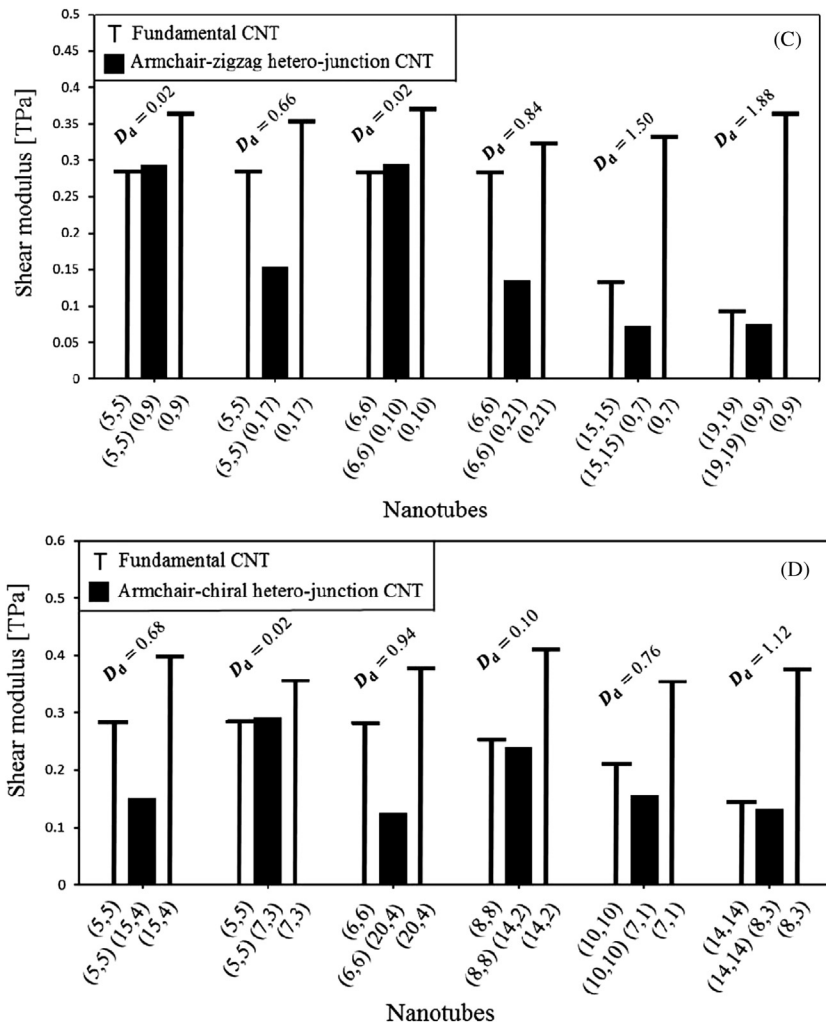


Figure 4.5 (Continued).

FEM was broadly employed by Ghavamian et al. [2,53] to simulate and characterize homogenous SW- and MWCNTs as well as hetero-junction CNTs in their defect-free and atomically defective forms with different percentages of random distribution of the atomic defects, i.e., silicon impurities, vacancies, and perturbation. For such a modeling, a cylinder-shaped truss structure, constructed of 1D beam elements (representing C–C bonds), was simulated and the corresponding materials and geometric properties (expressed in Table 4.1) were introduced to the

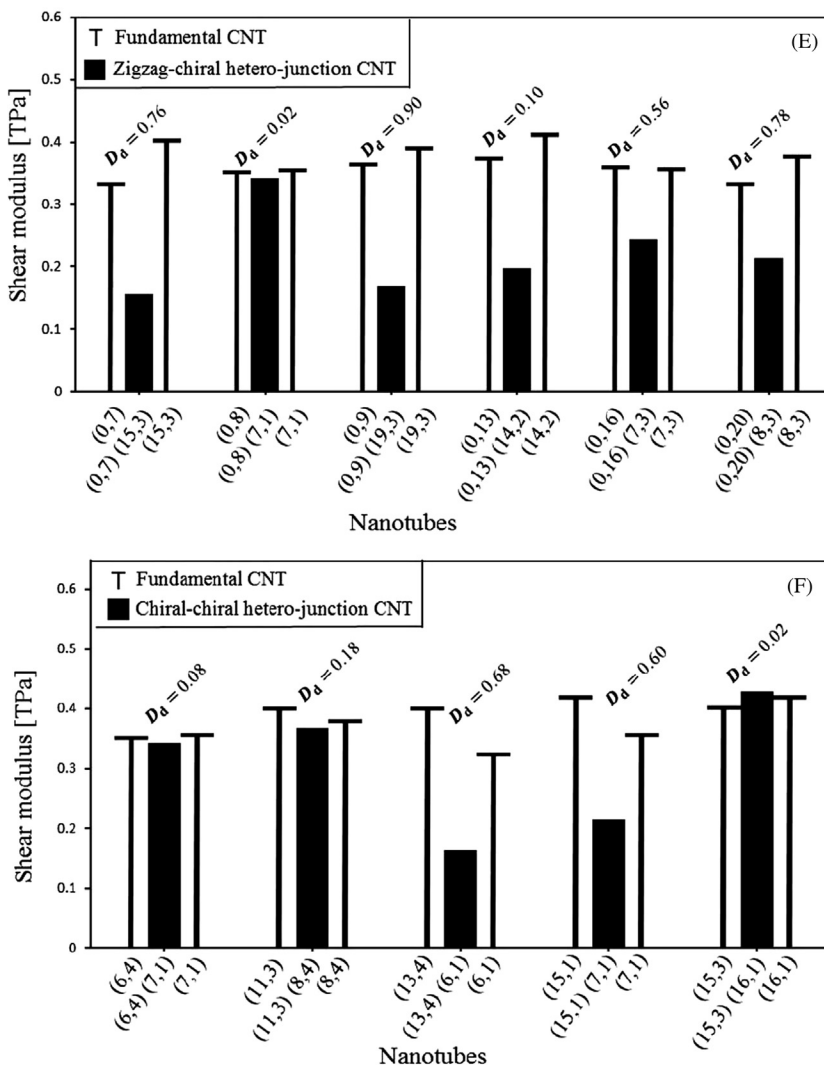


Figure 4.5 (Continued).

elements and eventually, their tensile, torsion, buckling, and vibrational properties were evaluated under the corresponding computer-simulated mechanical tests.

In the case of straight homogeneous CNTs, they reported a slight increase up to a converged value of about 1.05 TPa for the Young's modulus of CNTs by an increase in the number of their walls. However, the shear modulus, obtained from torsion tests, varied in the range of 0.07 to 0.38 TPa and demonstrated an inverse correlation to the increase in the number of CNTs' walls. A parabolic increase was

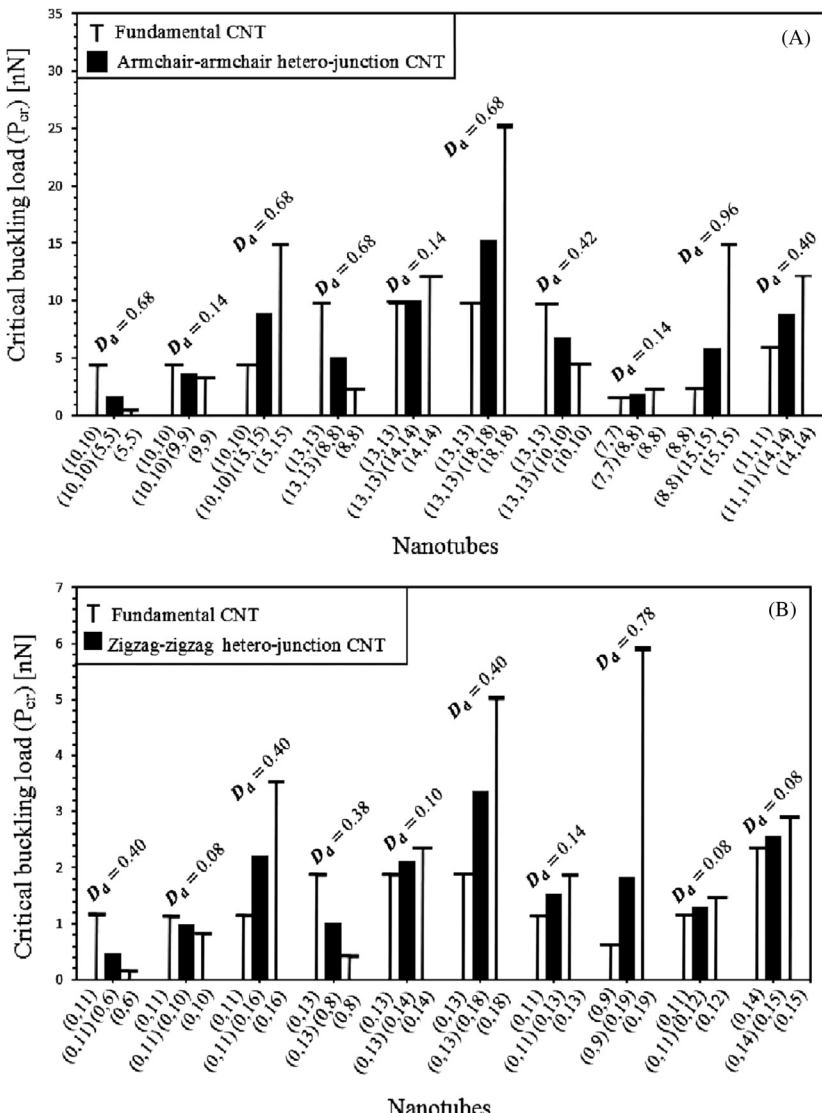


Figure 4.6 (A)–(F) Critical buckling load of hetero-junction and homogeneous CNTs.
Source: Adapted from [219].

also revealed in the critical buckling load of CNTs as a result of increasing their wall number [49,60,149,150]. Ghavamian and his colleagues also discovered that CNTs are anisotropic materials and therefore, their shear modulus can only be predicted via a pure torsion test [149]. With regards to atomically defective straight

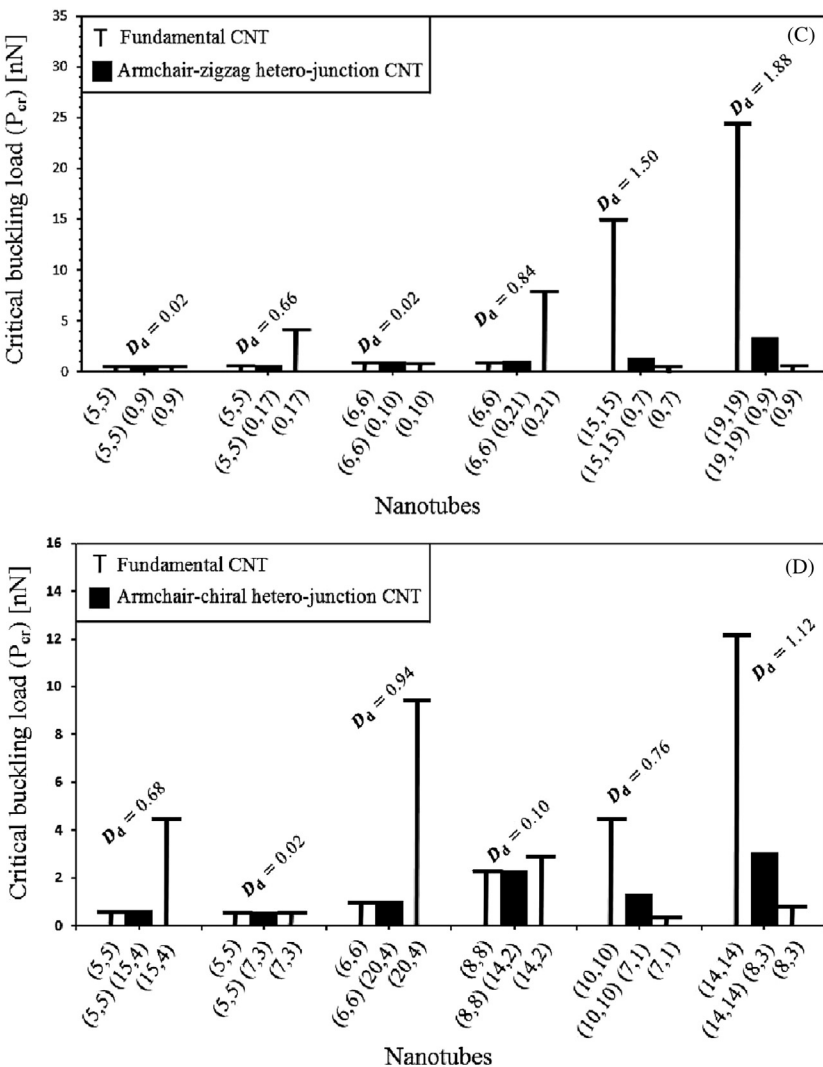
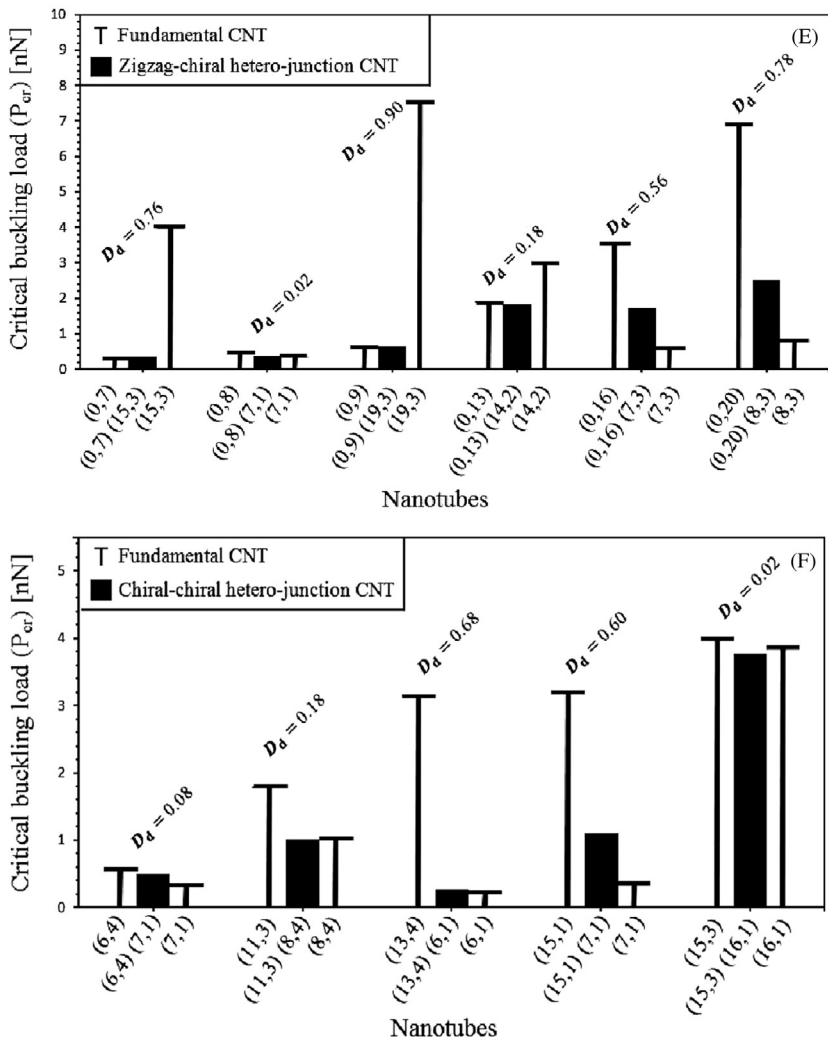


Figure 4.6 (Continued).

CNTs, they pointed out that any atomic defect type in the CNT structures decreases their mechanical strength and for the first time, proposed mathematical relations for the prediction of such a decrease in terms of the percentage of the atomic defect. Their results illustrated a linear decrease for Si-doping and carbon vacancy which could be expressed by Eq. (4.6). However, a parabolic decreasing trend was observed for the perturbation that is presented by Eq. (4.7).

**Figure 4.6** (Continued).

$$LC_{MQ} = a \times p, \quad (4.6)$$

$$NLC_{MQ} = a \times p + b \times p^2. \quad (4.7)$$

In Eqs. (4.6) and (4.7), LC_{MQ} and NLC_{MQ} are, respectively, linear and nonlinear change in the mechanical quantity, i.e., Young's modulus, critical buckling load, or natural frequency as a result of the atomic defect, and P is the percentage of the atomic defect in the CNT structure. Based on the results, the coefficient a for Young's modulus case, was obtained -1.88239 ± 0.050069 and -7.69879 ± 0.606014 for

Si-doping and carbon vacancy, respectively. This coefficient was also obtained for the critical buckling load case equal to -1.651587 ± 0.10534 and -8.429947 ± 1.544611 for Si-doping and carbon vacancy, respectively. Likewise, the value of -0.99801 ± 0.073892 was acquired for Si-doping as well as -5.23645 ± 0.292813 (for SWCNTs) and -3.25779 ± 0.357346 (for MWCNTs) for carbon vacancy in case of natural frequency of defective CNTs. For perturbed CNTs, the coefficients a and b in Eq. (4.7) were obtained -0.05034 ± 0.027558 and -0.01455 ± 0.002267 , respectively for Young's modulus case, -0.021917 ± 0.002504 and 0.023887 ± 0.021155 for critical buckling case and, -0.01289 ± 0.000832 and -0.0033 ± 0.009755 for natural frequency case. In the shear modulus case, although Si-doping led to lower torsional strength of these homogenous CNTs, no particular exact trend was observed to express such a decrease [49,60,149,150].

Later on, Ghavamian and Öchsner [219] applied the same approach for the mechanical characterization of a considerable number of defect-free and atomically defective hetero-junction CNTs with all connection types. In case of the influence of Stone–Wales defect, it was learned that such a defect clearly reduces the tensile and shear moduli of hetero-junction CNTs, compared with their constructive homogeneous tubes moduli, as shown in Figs. 4.4 and 4.5 where D_d is the difference between the diameter of constructive homogenous wider and thinner tubes of hetero-junction CNTs. However, in their buckling case, it was observed that the critical buckling loads of hetero-junction CNTs lies in the range of the buckling loads of their corresponding constructive homogenous tubes, as illustrated in Fig. 4.6. Moreover, among different hetero-junction CNTs, the lowest mechanical stability was observed in armchair–zigzag hetero-junction CNTs while the Young's modulus was observed at its maximum value for armchair–armchair and zigzag–zigzag models as well as the maximum shear modulus and critical buckling load, appearing for the CNTs with zigzag–zigzag and armchair–armchair connections, respectively.

Like defective homogeneous CNTs, it was observed that not only the atomically defective hetero-junction CNTs with Si-doping and carbon vacancies encountered a decrease in their mechanical strength as a result of defects, but also they demonstrated a linear decreasing trend in their mechanical properties which could be expressed by Eq. (4.6), where for these CNT types, the coefficient a was obtained -1.59 ± 0.39 , -1.10 ± 0.26 , and -1.76 ± 0.52 for prediction of the Si-doping-related decrease in their Young's modulus, shear modulus, and critical buckling loads, respectively, and the values of -8.17 ± 1.98 , -10.03 ± 2.78 , and -11.58 ± 1.98 for the a coefficient, regarding carbon vacancy defects [62,75].

4.5 Summary and outlook

4.5.1 Current theoretical and experimental findings

In summary, a collection of different concepts, i.e., synthesis and atomic structure, defects and modifications, characterization and properties, and applications as well

as a brief literature review, pertaining to the CNTs was discussed in this chapter with the focus on various defect types in the structure of these nanomaterials. According to what has been discussed, there are numerous techniques for the synthesis of CNTs which are different and comparable, based on their efficiency, costs, yields, and the industrial requirements. However, the experimental observations show that the produced CNTs are not defect-free and involve different types of defects and thus, they might be exposed to purification to remove redundant impurities and by-products and/or a functionalization process by which particular structural or atomic defects are introduced to the CNTs to tune their properties for their efficient functionalities in various applications from energy storing, gas detection, and materials reinforcement to drug delivery and molecules transportation. Among different impurities for the functionalization of the CNTs, nitrogen and phosphorus were referred to as popular candidates for overcoming the CNTs inertness and increasing their chemical reactivity, as well as enhancing their conductivity. Boron-doping, not only showed a similar ability to improve electrical conductivity and capacitance of CNTs, but also increases the environmental resistance of CNTs with regards to oxidization. On the other hand, Si-CNTs not only overtakes in the chemical reactivity, compared to the undoped or B-, N- or P-doped CNTs, but also appeared to be considerably applicable in the fabrication of CNT-based nanodevices that are designed to operate in harsh environments. Welding two or more CNTs with exciting electrical properties was another instance of CNTs' structural functionalization for producing hetero-junctions and molecular junctions to be employed as new generation of solar cells and multi-terminal devices, respectively.

Although appropriate chemical modification of CNTs has demonstrated improvement in their solubility, dispersion, and bonding with hosting matrix and thus, an increase in the mechanical strength of CNT-reinforced nanocomposite, both the experimental and theoretical investigations are in agreement that all of these modifications should still be treated as structural defects as they substantially decrease the stiffness and mechanical stability of individual CNTs. Si-doping and vacancies linearly and perturbation parabolically reduced the mechanical strength of CNTs. Stone-Wales defects result in lower tensile and torsion moduli of hetero-junction CNTs while such a defect drops the critical buckling load and natural frequency of hetero-junction CNTs in ranges below those for their constructive homogeneous tubes.

4.5.2 *Novel pathways for carbon device fabrication*

Even though invaluable efforts have been made in the investigation of the properties of CNTs, it is fair to say that only the very tip of the iceberg has been addressed. The concerns correspond to the costs and efficiency of the CNTs synthesis; the purification and functionalization process also necessitates such process optimization. On the other hand, although the theoretical characterization techniques anticipate the properties and behavior of CNTs in many complicated conditions with noticeable accuracy, as yet there are many limitations in the required experimental tools and technology to certainly validate the theoretical predictions. The solubility of CNTs and their dispersion as reinforcement in the structure of

nanocomposites is also another aspect of these nanomaterials to be enhanced. Despite the biomedical application potential of CNTs, the toxicity and the level of biocompatibility of CNTs has still remained a crucial argument for further and more conclusive investigations. Finally, with respect to high stiffness and other unique mechanical properties of CNTs, the establishment of a data base which present the mechanical properties of CNTs in terms of concentration and type of defects, temperature, chemical environment, presence of chemical functionalities, cycling of load, lifetime etc. seems to be necessary and demanded.

Acknowledgement

The authors acknowledge the funding provided by the Australian Government Research Training Program Scholarship.

References

- [1] Iijima S. Helical microtubules of graphitic carbon. *Nature* 1991;354:56–8.
- [2] Ghavamian A, Öchsner A. Influence of atomic defects on the mechanical properties of carbon nanotubes. In: Aliofkhazraei M, editor. *Handbook of Functional Nanomaterials*. United States: Nova publishers; 2014. p. 415–32.
- [3] Iijima S, Brabec Ch, Maiti A, Bernhole J. Structural flexibility of carbon nanotubes. *J Phys Chem* 1996;104:2089–92.
- [4] Rahmandoust M, Öchsner A. On finite element modeling of single and multi-walled carbon nanotubes. *J Nanosci Nanotechnol* 2012;12:8129–36.
- [5] Kantamneni H, Gollakota A. Carbon nanotubes based systems for targeted drug delivery : a review. *Int J Eng Res Technol* 2013;2:1–8.
- [6] Rümmeli MH, Bachmatiuk A, Börrnert F, Schäffel F, Ibrahim I, Cendrowski K, et al. Synthesis of carbon nanotubes with and without catalyst particles. *Nanoscale Res Lett* 2011;6:303–12.
- [7] Qi X, Xu J, Hu Q, Deng Y, Xie R, Jiang Y, et al. Metal-free carbon nanotubes: synthesis, and enhanced intrinsic microwave absorption properties. *Sci Rep* 2016;6:1–11.
- [8] Shi K, Yan J, Lester E, Wu T. Catalyst-Free Synthesis of multiwalled carbon nanotubes via microwave-induced processing of biomass. *Ind Eng Chem Res* 2014;53:15012–19.
- [9] Saito Y, Inagaki M. Yield of fullerenes generated by contact arc method under He and Ar-dependence on carbon nanotube. *Chem Phys Lett* 1992;200:643–8.
- [10] Isaacs JA, Tanwani A, Healy ML, Dahlben LJ. Economic assessment of single-walled carbon nanotube processes. *J Nanopart Res* 2010;12:551–62.
- [11] Ebbesen TW, Ajayan PM. Large-scale synthesis of carbon nanotubes. *Nature* 1992;358:220–2.
- [12] Guo T, Nikolaev P, Thess A, Colbert DT, Smalley RE. Catalytic growth of single-walled manotubes by laser vaporization. *Chem Phys Lett* 1995;243:49–54.
- [13] Journet C, Maser WK, Bernier P, Loiseau A, Lamy de la Chapelle M, Lefrant S, et al. Large-scale production of single-walled carbon nanotubes by the electric-arc technique. *Nature* 1997;388:756–8.

- [14] Jost O, Gorbunov A, Liu X, Pompe W, Fink J. Single-walled carbon nanotube diameter. *J Nanosci Nanotechnol* 2004;4:433–40.
- [15] Walker PL, Rakiszawski JF, Imperial GR. Carbon formation from carbon monoxide-hydrogen mixtures over iron catalysts.I. properties of carbon formed. *J Phys Chem* 1959;63:133–40.
- [16] José-Yacamán M, Miki-Yoshida M, Rendón L, Santiesteban JG. Catalytic growth of carbon microtubules with fullerene structure. *Appl Phys Lett* 1993;62:657–9.
- [17] Moore V, Strano M, Haroz E, Hauge R. R. smalley, Individually suspended single-walled carbon nanotubes in various surfactants. *Nano Lett* 2003;3:1379–82.
- [18] Endo M. Grow carbon fibers in the vapor phase. *Chemtech* September 1988;18:568–76.
- [19] Rafique MMA, Iqbal J. Production of carbon nanotubes by different routes A review. *J Encapsulat Adsorpt Sci* 2011;1:29–34.
- [20] Height MJ, Howard JB, Tester JW, Sande JBV. Flame synthesis of single-walled carbon nanotubes. *Carbon* 2004;42:2295–307.
- [21] Akiladevi D, Basak S. Carbon nanotubes (CNTs) production, characterization and its applications. *Int J Adv Pharm Sci* 2010;1:187–95.
- [22] Rinaldi A, Zhang J, Frank B, Su DS, Abd Hamid SB, Schlägl R. Oxidative purification of carbon nanotubes and its impact on catalytic performance in oxidative dehydrogenation reactions. *ChemSusChem* 2010;3:254–60.
- [23] Ismail AF, Goh PS, Tee JC, Sanip SM, Aziz M. A review of purification techniques for Carbon nanotubes. *NANO* 2008;3:127–43.
- [24] Martínez MT, Callejas MA, Benito AM, Cochet M, Seeger T, Ansón A, et al. Modifications of single-wall carbon nanotubes upon oxidative purification treatments. *Nanotechnology* 2003;14:691–5.
- [25] Borowiak-Palen E, Pichler T, Liu X, Knupfer M, Graff A, Jost O, et al. Reduced diameter distribution of single-wall carbon nanotubes by selective oxidation. *Chem Phys Lett* 2002;363:567–72.
- [26] Kajlura H, Tsutsui S, Huang HJ, Murakami Y. High quality single-walled carbon nanotubes from arc-produced soot. *Chemical Physics Letters* 2002;364:586–92.
- [27] Thien-Nga L, Hernadi K, Ljubovic E, Garaj S, Forro L. Mechanical purification of single-walled carbon nanotube bundles from catalytic particles. *Nano Lett* 2002;2:1349–52.
- [28] Hou PX, Liu C, Tong Y, Liu M, Cheng MH. Purification of single-walled carbon nanotubes synthesized by the hydrogen arc-discharge method. *J Mater Res* 2001;16:2526–9.
- [29] Chiang IW, Brinson BE, Huang AY, Willis PA, Bronikowski MJ, Margrave JL, et al. Purification and characterization of single-wall carbon nanotubes (SWNTs) obtained from the gas-phase decomposition of CO (HiPco process). *J Phys Chem B* 2001;105:8297–301.
- [30] Singh P, Campidelli S, Giordani S, Bonifazi D, Bianco A, Prato A. Organic functionalization and characterization of single-walled carbon nanotubes. *Chem Soc Rev* 2009;38:2214–30.
- [31] Hou PX, Liu C, Cheng HM. Purification of carbon nanotubes. *Carbon* 2008;46:2003–25.
- [32] Park YS, Choi YC, Kim KS, Chung DC, Bae DJ, An KH, et al. High yield purification of multiwalled carbon nanotubes by selective oxidation during thermal annealing. *Carbon* 2001;39:655–61.
- [33] Bandow S, Rao AM, Williams KA, Thess A, Smalley RE, Eklund PC. Purification of single-wall carbon nanotubes by microfiltration. *J Phys Chem B* 1997;101:8839–42.

- [34] Dyke CA, Tour JM. Covalent functionalization of single-walled carbon nanotubes for materials applications. *J Phys Chem A* 2004;108:11151–9.
- [35] Chavan R, Desai U, Mhatre P, Chinchole R. A review: carbon nanotubes. *Int J Pharm Sci Rev Res* 2012;13:125–34.
- [36] Li X, Wong SY, Tjiu WC, Lyons BP, Oh SA, He CB. Non-covalent functionalization of multi walled carbon nanotubes and their application for conductive composites. *Carbon* 2008;46:818–32.
- [37] Imani Yengejeh S, Akbar Zadeh M, Öchsner A. On the buckling behavior of connected carbon nanotubes with parallel longitudinal axes. *Appl Phys A* 2014;115:1335–44.
- [38] Treacy MMJ, Ebbesen TW, Gibson MJ. Exceptionally high Young's modulus observed for individual carbon nanotubes. *Nature* 1996;381:678–80.
- [39] Tans SJ, Verschueren ARM, Dekker C. Room-temperature transistor based on a single carbon nanotube. *Nature* 1998;393:49–52.
- [40] Friedman RS, McAlpine MC, Ricketts DS, Ham D, Lieber CM. Nanotechnology: high-speed integrated nanowire circuits. *Nature* 2005;434:1085.
- [41] Lee CJ, Kim DW, Lee TJ, Choi YC, Park YS, Kim WS, et al. Synthesis of uniformly distributed carbon nanotubes on a large area of Si substrates by thermal chemical vapor deposition. *Appl Phys Lett* 1999;75:1721–3.
- [42] Pancharal P, Wang ZL, Ugarte D, de Heer W. Electrostatic deflections and electromechanical resonances of carbon nanotubes. *Science* 1999;283:1513–16.
- [43] Kong J, Franklin NR, Zhou CW, Chapline MG, Peng S, Cho KJ, et al. Nanotube molecular wires as chemical sensors. *Science* 2000;287:622–5.
- [44] Wang QH, Yan M, Chang RPH. A nanotube-based field-emission flat panel display. *Appl Phys Lett* 1998;72:2912–13.
- [45] Kim P, Lieber CM. Nanotube nanotweezers. *Science* 1999;285:2148–50.
- [46] Dai H, Hafner JH, Rinzler AG, Cebert DT, Smalley RE. Nanotubes as nanoprobe in scanning probe microscopy. *Nature* 1996;384:147–50.
- [47] Dillon AC, Jones KM, Bekkedahl TA, Kiang CH, Bethune DS, Heben MJ. Storage of hydrogen in single-walled carbon nanotubes. *Nature* 1997;386:377–9.
- [48] Bianco BA, Kostarelos K, Prato M. Applications of carbon nanotubes in drug delivery. *Curr Opin Chem Biol* 2005;9:674–9.
- [49] Ghavamian A, Rahmandoust M, Öchsner A. A numerical evaluation of the influence of defects on the elastic modulus of single and multi-walled carbon nanotubes. *Comput Mater Sci* 2012;62:110–16.
- [50] T.R. Prabu, Finite element modeling of multi-walled carbon nanotube, B. Tech. Thesis, National Institute of Technology Rourkela, Orissa India, 2010.
- [51] Dunlap BI. Relating carbon tubules. *Phys Rev B* 1994;49:5643–50.
- [52] Fejes D, Németh Z, Hernádi K. CVD synthesis of spiral carbon nanotubes over asymmetric catalytic particles. *React Kinet Catal Lett* 2009;96:397–404.
- [53] Ghavamian A, Rahmandoust M, Öchsner A. Numerical nanomechanics of perfect and defective hetero-junction CNTs. In: Silvestre N, editor. *Advanced Computational Nanomechanics*. United Kingdom: John Wiley & Sons; 2016. p. 147–74.
- [54] Terrones M, Banhart F, Grobert N, Charlier JC, Terrones H, Ajayan PM. Molecular junctions by joining single-walled carbon nanotubes. *Phys Rev Lett* 2002;89:075505-1-4.
- [55] Nath DCD, Sahajwalla V. Application of fly ash as a catalyst for synthesis of carbon nanotube ribbons. *J Hazard Mater* 2011;192:691–7.
- [56] Li Y, Mi R, Li S, Liu X, Ren W, Liu H, et al. Sulfur-nitrogen doped multi walled carbon nanotubes composite as a cathode material for lithium sulfur batteries. *Int J Hydro Energy* 2014;39:16073–80.

- [57] Yuan N, Bai H, Ma Y, Ji Y. First-principle simulations on silicon-doped armchair single-walled carbon nanotubes of various diameters. *Phys E* 2014;64:195–203.
- [58] Cheng Y, Tian Y, Fan X, Liu J, Yan C. Boron doped multi-walled carbon nanotubes as catalysts for oxygen reduction reaction and oxygen evolution reaction in alkaline media. *Electrochim Acta* 2014;143:291–6.
- [59] Collins PG. Defects and disorder in carbon nanotubes, Oxford Handbook of Nanoscience and Technology, Materials: Structures, Properties and Characterization. Techniques 2010;2:31.
- [60] Ghavamian A, Öchsner A. Numerical modeling of eigenmodes and eigenfrequencies of single- and multi-walled carbon nanotubes under the influence of atomic defects. *Comput Mater Sci* 2013;72:42–8.
- [61] Ponomareva I, Chernozatonskii LA, Andriotis AN, Menon M. Formation pathways for single-wall carbon nanotube multiterminal junctions. *New J Phys* 2003;5:119.1–119.12.
- [62] Ghavamian A, Andriyana A, Chin AB, Öchsner A. Numerical investigation on the influence of atomic defects on the tensile and torsional behavior of hetero-junction carbon nanotubes. *Mater Chem Phys* 2015;164:122–37.
- [63] Tans SJ, Devoret MH, Dai H, Tess A, Smalley RE, Gerligs LJ, et al. Individual single-wall carbon nanotubes as quantum wires. *Nature* 1997;386:474–7.
- [64] Terrones M, Souza Filho AG, Rao AM. Doped carbon nanotubes: synthesis, characterization and applications, Carbon nanotubes Topics Applied Physics, 111. Berlin: Springer; 2008. p. 531–66.
- [65] Bian R, Jingxiang Z, Honggang F. Silicon–doping in carbon nanotubes: formation energies, electronic structures, and chemical reactivity. *J Mol Model* 2013;19:1667–75.
- [66] Ayala P, Arenal R, Rümmeli M, Rubio A, Pichler T. The doping of carbon nanotubes with nitrogen and their potential applications. *Carbon* 2010;48:575–86.
- [67] Jang JW, Cheol EL. Structural study of nitrogen-doping effects in bamboo-shaped multi-walled carbon nanotubes. *Appl Phys Lett* 2004;84:2877–9.
- [68] Cruz-Silva E, Pez-Urias FL, Munoz-Sandoval E, Sumpter BG, Terrones H, Charlier JC, et al. Electronic transport and mechanical properties of phosphorus- and phosphorus_nitrogen-doped carbon nanotubes. *ACS Nano* 2009;3:1913–21.
- [69] Larrude DG, Maia da Costa MEH, Monteiro FH, Pinto AL, Freire FL. Characterization of phosphorus-doped multiwalled carbon nanotubes. *J Appl Phys* 2012;111:064315-1-6.
- [70] Yeh MH, Lin LY, Lia TJ, Leub YA, Chenc GL, Tiend TC, et al. Synthesis of boron–doped multi–walled carbon nanotubes by an ammonia–assisted substitution reaction for applying in supercapacitors. *Energy Proc* 2014;61:1764–7.
- [71] Handuja S, Srivastava P, Vankar VD. Structural modification in carbon nanotubes by boron incorporation. *Nanoscale Res Lett* 2009;4:789–93.
- [72] Yeom DY, Jeon W, Tu NDK, Yeo SY, Lee SS, Sung BJ, et al. High-concentration boron doping of graphene nanoplatelets by simple thermal annealing and their supercapacitive properties. *Sci Rep* 2015;5:1–10.
- [73] Gowri sankar PA, Udhayakumar K. Electronic properties of boron and silicon doped (10, 0) zigzag single-walled carbon nanotube upon gas molecular adsorption: a DFT comparative study. *J Nanomater* 2013;2013:1–12.
- [74] Baierle RJ, Fagan SB, Mota R, da Silva AJR, Fazzio A. Electronic and structural properties of silicon-doped carbon nanotubes. *Phys Rev B* 2001;64 085413-1-4.
- [75] Ghavamian A, Öchsner A. On the buckling behavior of perfect and atomically defective hetero-junction carbon nanotubes. *Mech Adv Mater Struct* 2016; ISSN: 1537-6494.

- [76] Chico L, Crespi VH, Benedict LX, Louie SG, Cohen ML. Pure carbon nanoscale devices: nanotube heterojunctions. *Phys Rev Lett* 1996;76:971–4.
- [77] Wang H, Bai X, Wei J, Li P, Jia Y, Zhu H, et al. Preparation of CuI particles and their applications in carbon nanotube-Si heterojunction solar cells mater. *Mater Lett* 2012;79:106–8.
- [78] Jia Y, Cao A, Bai X, Li Z, Zhang L, Guo N, et al. Achieving high efficiency silicon-carbon nanotube heterojunction solar cells by acid doping. *Nano Lett* 2011;11:1901–5.
- [79] Slaoui A, Collins RT. Advanced inorganic materials for photovoltaics. *MRS Bull* 2007;32:211–18.
- [80] Jia Y, Wei J, Wang K, Cao A, Shu Q, Gui X, et al. Nanotube–silicon heterojunction solar cells. *Adv Mater* 2008;20:4594–8.
- [81] Gai PL, Stephan O, McGuire K, Rao AM, Dresselhaus MS, Dresselhaus G, et al. Structural systematics in boron-doped single wall carbon nanotubes. *J Mater Chem* 2004;14:669–75.
- [82] Echlin P. Ed. *Handbook of Sample Preparation for Scanning Electron Microscopy and x-ray Microanalysis*, 330. Springer; 2009. ISBN 978-0-387-85731-2.
- [83] Goldstein J, Newbury D, Joy D, Lyman C, Echlin P, Lifshin F, et al. *Scanning Electron Microscopy and X-ray Microanalysis*. 3rd Ed. Springer; 2003.
- [84] Gommes C, Blacher S, Masenelli-Varlot K, Bossuot C, McRae E, Fonseca A, et al. Image analysis characterization of multi-walled carbon Nanotubes. *Carbon* 2003;41:2561–72.
- [85] Kiang C, Endo M, Ajayan P, Dresselhaus G, Dresselhaus M. Size effects in carbon nanotubes. *Phys Rev Lett* 1998;81:1869–72.
- [86] Charlier A, McRae E, Heyd R, Charlier M, Moretti D. Classification for double-walled carbon nanotubes. *Carbon* 1999;37:1779–83.
- [87] Cowley J, Sundell F. Nanodiffraction and dark-field STEM characterization of single-walled carbon nanotube ropes. *Ultramicroscopy* 1997;68:1–12.
- [88] He R, Jin H, Zhu J, Yan Y, Chen X. Physical and electronic structure in carbon nanotubes. *Chem Phys Lett* 1998;298:170–6.
- [89] Qin L, Iijima S, Kataura H, Maniwa Y, Suzuki S, Achiba Y. Helicity and packing of single-walled carbon nanotubes studied by electron nanodiffraction. *Chem Phys Lett* 1997;268:101–6.
- [90] Bernaerts D, Zettl A, Chopra N, Thess A, Smalley R. Electron diffraction study of single-wall carbon nanotubes. *Solid State Commun* 1998;105:145–9.
- [91] Wildoer J, Venema L, Rinzler A, Smalley R, Dekker C. Electronic structure of atomically resolved carbon nanotubes. *Nature* 1998;391:59–62.
- [92] Ichimura K, Osawa M, Nomura K, Kataura H, Maniwa Y, Suzuki S, et al. Tunneling spectroscopy on carbon nanotubes using STM. *Phys B* 2002;323:230–2.
- [93] Lin N, Ding J, Yang S, Cue N. Scanning tunneling microscopy and spectroscopy of a carbon nanotube. *Carbon* 1996;34:1295–7.
- [94] Hassanien A, Tokumoto M. The electronic properties of suspended single wall carbon nanotubes. *Carbon* 2004;42:2649–53.
- [95] Obraztsova E, Yurov V, Shevluga V, Baranovsky R, Nalimova V, Kuznetsov V, et al. Structural investigations of close-packed single-wall carbon nanotube material. *NanoStruct Mater* 1999;11:295–306.
- [96] Kim P, Odom T, Huang J, Lieber C. STM study of single-walled carbon nanotubes. *Carbon* 2000;38:1741–4.
- [97] Bellucci S, Gaggiotti G, Marchetti M, Micciulla F, Mucciato R, Regi M. Atomic force microscopy characterization of carbon nanotubes. *J Phys* 2007;61:99–104.

- [98] Kim JS, Lee JH, Hong SU, Han WS, Kwack HS, Lee CW, et al. Formation of self-assembled InAs quantum dots on InAl(Ga)As/InP and effects of a thin GaAs layer. *J Cryst Growth* 2003;259:252–6.
- [99] Kwon J, Hong J, Kim YS, Lee DY, Lee K, Lee S, et al. Atomic force microscope with improved scan accuracy, scan speed, and optical vision. *Rev Sci Inst* 2003;74:4378–83.
- [100] Oh S, Hyon C, Sull S, Hwang S. Detection and volume estimation of semiconductor quantum dots from atomic force microscope images. *Rev Sci Inst* 2003;74:4687–95.
- [101] Hemraj-Benny T, Banerjee S, Sambasivan S, Balasubramanian M, Fischer DA, Eres G, et al. Near-edge X-ray absorption fine structure spectroscopy as a tool for investigating nanomaterials. *Wiley* 2006;2:26–35.
- [102] Yano J, Yachandra VK. X-ray absorption spectroscopy. *Photosynth Res* 2009;102:241–54.
- [103] Lee V, Whittaker L, Jaye C, Baroudi KM, Fischer DA, Banerjee S. Large-area chemically modified graphene films: electrophoretic deposition and characterization by soft x-ray absorption spectroscopy. *Chem Mater* 2009;21:3905–16.
- [104] D. Spiga, A. Mirone, G. Pareschi, R. Canestrari, V. Cotroneo, C. Ferrari, et al., Characterization of multilayer stack parameters from X-ray reflectivity data using the PPM program: measurements and comparison with TEM results, *Proceedings of the SPIE, Space Telescopes and Instrumentation II: Ultraviolet to Gamma Ray* 6266 (2006) 626616.
- [105] Zhu W, Miser D, Chan W, Hajaligol M. Characterization of multiwalled carbon nanotubes prepared by carbon arc cathode deposit. *Mater Chem Phys* 2003;82:638–47.
- [106] Belin T, Epron F. Characterization methods of carbon nanotubes: a review. *Mater Sci Eng B* 2005;119:105–18.
- [107] Engelhard MH, Droubay TC, Du Y. *X-Ray Photoelectron Spectroscopy Applications*. 3rd edition Oxford, United Kingdom: Academic Press; 2017. p. 716–724 p.
- [108] Droppa R, Hammer P, Carvalho A, Dos Santos M, Alvarez F. Incorporation of nitrogen in carbon nanotubes,. *J Noncryst Solids* 2002;299–302:874–9.
- [109] Hammer P, Victoria N, Alvarez F. Effects of increasing nitrogen concentration on the structure of carbon nitride films deposited by ion beam assisted deposition. *J Vac Sci Technol A* 2000;18:2277–87.
- [110] Ouyang M, Huang JL, Cheung CL, Lieber CM. Energy gaps in "metallic" single-walled carbon nanotubes. *Science* 2001;292:702–5.
- [111] Lauret JS, Voisin C, Cassabois G, Roussignol P, Delalande C, Filoromo A, et al. Bandgap photoluminescence of semiconducting single-wall carbon nanotubes. *Phys E* 2004;21:1057–60.
- [112] Liu X, Pichler T, Knupfer M, Golden MS, Fink J, Kataura H, et al. Detailed analysis of the mean diameter and diameter distribution of single-wall carbon nanotubes from their optical response. *Phys Rev B* 2002;66:045411–0454118.
- [113] Lefebvre J, Fraser JM, Homma Y, Finnie P. Photoluminescence from single-walled carbon nanotubes: a comparison between suspended and micelle-encapsulated nanotubes. *Appl Phys A* 2004;78:1107–10.
- [114] Weisman RB, Bachilo SM, Tsymbal斯基 D. Fluorescence spectroscopy of single-walled carbon nanotubes in aqueous suspension. *Appl Phys A* 2004;78:1111–16.
- [115] O'Connell MJ, Bachilo SM, Huffman CB, Moore VC, Strano MS, Haroz EH, et al. Band gap fluorescence from individual single-walled carbon nanotubes. *Science* 2002;297:593–6.

- [116] Lebedkin S, Hennrich F, Skipa T, Kappes MM. Near-infrared photoluminescence of single-walled carbon nanotubes prepared by the laser vaporization method. *J Phys Chem B* 2003;107:19491956.
- [117] Miyauchi Y, Chiashi S, Murakami Y, Hayashida Y, Maruyama S. Fluorescence spectroscopy of single-walled carbon nanotubes synthesized from alcohol. *Chem Phys Lett* 2004;387:198–203.
- [118] Kuhlmann U, Jantoljak H, Pfander M, Bernier P, Journet C, Thomsen C. Infrared active phonons in single-walled carbon nanotubes. *Chem Phys Lett* 1998;294:237–40.
- [119] Kuzmany H, Burger B, Thess A, Smalley R. Vibrational spectra of single wall carbon,. *Nanotubescarbon* 1998;36:709–12.
- [120] Kastner J, Pichler T, Kuzmany H, Curran S, Blau W, Weldon DN, et al. Resonance raman and infrared spectroscopy of carbon nanotubes. *Chem Phys Lett* 1994;221:53–8.
- [121] Eklund P, Holden J, Jishi R. Vibrational modes of carbon nanotubes; spectroscopy and theory. *Carbon* 1995;33:959–72.
- [122] Saito R, Matsushige K, Tanaka K. Chemical treatment and modification of multi-walled carbon nanotubes. *Physica B* 2002;323:280–3.
- [123] He B, Sun W, Wang M, Liu S, Shen Z. Preparation and characterization of a series of novel complexes by single-walled carbon nanotubes (SWNTs) connected poly(amic acid) containing bithiazole ring. *Mater Chem Phys* 2004;84:140–5.
- [124] Costa S, Borowiak-Palen E, Kruszyńska M, Bachmatiuk A, Kaleńczuk RJ. Characterization of carbon nanotubes by Raman spectroscopy. *Mat Sci Poland* 2008;26:433–41.
- [125] Antunes EF, Lobo AO, Corat EJ, Trava-Airoldi VJ, Martin AA, Veríssimo C. Comparative study of first- and second-order Raman spectra of MWCNT at visible and infrared laser excitation. *Carbon* 2006;44:2202–11.
- [126] Ritter U, Scharff P, Siegmund C, Dmytrenko OP, Kulish NP, Prylutskyy YI, Belyi NM. Radiation damage to multi-walled carbon nanotubes and their Raman vibrational modes. *Carbon* 2006;44:2694–700.
- [127] Takeda N, Murakoshi K. Characteristics of the Raman spectra of single-walled carbon nanotube bundles under electrochemical potential control. *Anal Bioanal Chem* 2007;388:103–8.
- [128] Doorn SK, Heller DA, Barone PW, Usrey ML, Strano MS. Resonant Raman excitation profiles of individually dispersed single walled carbon nanotubes in solution. *Appl Phys A* 2004;78:1147–55.
- [129] Dresselhaus MS, Dresselhaus G, Jorio A, Souza Filho AG, Pimenta MA, Saito R. Single nanotube Raman spectroscopy. *Acc Chem Res* 2002;35:1070–8.
- [130] Dresselhaus MS, Dresselhaus G, Jorio A, Souza Filho AG, Saito R. Raman spectroscopy on isolated single wall carbon nanotubes. *Carbon* 2002;40:2043–61.
- [131] Dresselhaus MS, Jorio A, Souza Filho AG, Dresselhaus G, Saito R. Raman spectroscopy on one isolated carbon nanotube. *Physica B* 2002;323:15–20.
- [132] Dresselhaus MS, Dresselhaus G, Saito R, Jorio A. Raman spectroscopy of carbon nanotubes. *Phys Rep* 2005;409:47–99.
- [133] Zhang HB, Lin GD, Zhou ZH, Dong X, Chen T. Raman spectra of MWCNTs and MWCNT-based H₂ adsorbing system. *Carbon* 2002;40:2429–36.
- [134] Arepalli S, Nikolaev P, Gorelik O, Hadjiev V, Holmes W, Files B, Yowell L. Protocol for the characterization of single-wall carbon nanotube material quality. *Carbon* 2004;42:1783–91.

- [135] Ferrari A, Robertson J. Interpretation of Raman spectra of disordered and amorphous carbon. *Physical Review B* 2000;61:14095–107.
- [136] Assadi MHN, Hanaor DA. Theoretical study on copper's energetics and magnetism in TiO₂ polymorphs. *J Appl Phys* 2013;113:233913.
- [137] Jensen F. Introduction to Computational Chemistry. New York: Wiley; 1999.
- [138] Szabo A, Ostlund NS. Modern Quantum Chemistry. Dover Publications; 1996.
- [139] Parr RG, Yang W. Density Functional Theory of Atoms and Molecules. Oxford: Oxford University Press; 1989.
- [140] Hohenberg P, Kohn W. Inhomogeneous electron gas. *Phys Rev B* 1964;136:864–71.
- [141] Chen X, Cao G. A structural mechanics study of single-walled carbon nanotubes generalized from atomistic simulation. *Nanotechnology* 2006;17:1004–15.
- [142] Tserpes KI, Papanikos P. Finite element modeling of single-walled carbon nanotubes. *Composites* 2005;36:468–77.
- [143] Brenner DW. Empirical potential for hydrocarbons for use in simulating the chemical vapor deposition of diamond films. *Phys Rev B* 1990;42:9458–71.
- [144] Girifalco LA. Molecular properties of fullerene in the gas and solid phases. *Phys Chem* 1992;96:858–61.
- [145] Alder BJ, Wainwright TE. Studies in molecular dynamics. I. general metho. *J Chem Phys* 1959;31:459–66.
- [146] Yao Z, Zhu CC, Cheng M, Liu J. Mechanical properties of carbon nanotubes by molecular dynamics simulation. *Comput Mater Sci* 2001;22:180–4.
- [147] Logan DL. A First Course in the Finite Element Method. Cengage Learning; 2011.
- [148] Silvestre N, Wang CM, Zhang YY, Xiang Y. Sanders shell model for buckling of single-walled carbon nanotubes with small aspect ratio. *Composite Struct* 2011;93:1683–91.
- [149] Ghavamian A, Rahmandoust M, Öchsner A. On the determination of the shear modulus of carbon nanotubes. *Composites* 2013;44:52–9.
- [150] Ghavamian A, Öchsner A. Numerical investigation on the influence of defects on the buckling behavior of single- and multi-walled carbon nanotubes. *Phys E* 2012;46:241–9.
- [151] Lu JP. Elastic properties of carbon nanotubes and nanoropes. *Phys Rev Lett* 1997;79:1297–300.
- [152] Salvetat JP, Bonard JM, Thomson NH, Kulik AJ, Forró L, Benoit W, et al. Mechanical properties of carbon nanotubes. *Appl Phys A* 1999;69:255–60.
- [153] Song YS, Youn JR. Influence of dispersion states of carbon nanotubes on physical properties of epoxy nanocomposites. *Carbon* 2005;43:1378–85.
- [154] Shanmugharaj AM, Bae JH, Lee KY, Noh WH, Lee SH, Ryu SH. Physical and chemical characteristics of multiwalled carbon nanotubes functionalized with aminosilane and its influence on the properties of natural rubber composites. *Composites Sci Technol* 2007;67:1813–22.
- [155] Zhu J, Kim JD, Peng H, Margrave JL, Khabashesku VN, Barrera EV. Improving the dispersion and integration of single-walled carbon nanotubes in epoxy composites through functionalization. *Nano Lett* 2003;3:1107–13.
- [156] Paiva MC, Zhou B, Fernando KAS, Lin Y, Kennedy JM, Sun YP. Mechanical and morphological characterization of polymer–carbon nanocomposites from functionalized carbon nanotubes. *Carbon* 2004;42:2849–54.
- [157] Mitchell CA, Bahr JL, Arepalli S, Tour JM, Krishnamoorti R. Dispersion of functionalized carbon nanotubes in polystyrene. *Macromolecules* 2002;35:8825–30.
- [158] Dai H, Wong EW, Liebert CM. Probing electrical transport in nanomaterials: conductivity of individual carbon nanotubes. *Science* 1996;272:1861.

- [159] Xie S, Li W, Pan Z, Chang B, Sun L. Mechanical and physical properties on carbon nanotube. *J Phys Chem Solids* 2000;61:1153–8.
- [160] Ruoff RS, Lorents DC. Mechanical and thermal properties of carbon nanotubes. *Carbon* 1995;33:925–30.
- [161] Sun YP, Huang W, Lin Y, Fu K, Kitaygorodskiy A, Riddle LA, et al. Soluble dendron-functionalized carbon nanotubes: preparation, characterization, and properties. *Chem Mater* 2001;13:2864–9.
- [162] Zeng H, Gao C, Yan D. Poly(ϵ -caprolactone)-functionalized carbon nanotubes and their biodegradation properties. *Adv Funct Mater* 2006;16:812–18.
- [163] Kong J, Chapline MG, Dai H. Functionalized carbon nanotubes for molecular hydrogen sensors. *Adv Mater* 2001;13:1384–6.
- [164] Sanip SM, Ismail AF, Goh PS, Soga T, Tanemura M, Yasuhiko H. Gas separation properties of functionalized carbon nanotubes mixed matrix membranes. *Sep Purif Technol* 2011;78:208–13.
- [165] Chen RJ, Zhang Y, Wang D, Dai H. Noncovalent sidewall functionalization of single-walled carbon nanotubes for protein immobilization. *J Am Chem Soc* 2001;123:3838–9.
- [166] Prato M, Kostarelos K, Bianco A. Functionalized carbon nanotubes in drug design and discovery. *Acc Chem Res* 2008;41:60–8.
- [167] Singh R, Pantarotto D, McCarthy D, Chaloin O, Hoebeke J, Partidos CD, et al. Binding and condensation of plasmid DNA onto functionalized carbon nanotubes: toward the construction of nanotube-based gene delivery vectors. *J Am Chem Soc* 2005;127:4388–96.
- [168] Hu H, Ni Y, Montana V, Haddon RC, Parpura V. Chemically functionalized carbon nanotubes as substrates for neuronal growth. *Nano Lett* 2004;4:507–11.
- [169] Charlier JC, Ebbesen TW, Ph. Lambin, Structural and electronic properties of pentagon-heptagon pair defects in carbon nanotubes. *Phys Rev B* 1995;53:11108–13.
- [170] Sánchez-Portal D, Artacho E, Soler JM. Ab initio structural, elastic, and vibrational properties of carbon nanotubes. *Phys Rev B* 1999;59:12678–88.
- [171] Ma Y, Lehtinen PO, Foster AS, Nieminen RM. Magnetic properties of vacancies in graphene and single-walled carbon nanotubes. *New J Phys* 2004;6:68.
- [172] Mirzaei M, Gulseren O. DFT studies of CNT–functionalized uracil-acetate. *Phys E* 2015;73:105–9.
- [173] Kinoshita Y, Murashima M, Kawachi M, Ohno N. First-principles study of mechanical properties of one-dimensional carbon nanotube intramolecular junctions. *Comput Mater Sci* 2013;70:1–7.
- [174] El-Barbary AA, Kamel MA, Eid KM, Taha HQ, Hassan MM. Mono-vacancy and B-doped defects in carbon heterojunction nanodevices. *Graphene* 2015;4:84–90.
- [175] Yakobson BI, Brabec CJ, Bernholc J. Structural mechanics of carbon nanotubes: from continuum elasticity to atomistic fracture. *J Comput Aided Mater Des* 1996;3:173–82.
- [176] Ru CQ. Effect of van der Waals forces on axial buckling of a double-walled carbon nanotube. *J Appl Phys* 2000;87:7227–31.
- [177] Silvestre N. On the accuracy of shell models for torsional buckling of carbon nanotubes. *Eur J Mech A/Solids* 2012;32:103–8.
- [178] Hu YG, Liew KM, Wang Q. Modeling of vibrations of carbon nanotubes. *Proc Eng* 2012;31:343–7.
- [179] Lu JM, Hwang CC, Kuo QY, Wang YC. Mechanical buckling of multi-walled carbon nanotubes: The effects of slenderness ratio. *Phys E* 2008;40:1305–8.

- [180] Liew KM, Wong CH, He XQ, Tan MJ, Meguid SA. Nanomechanics of single and multiwalled carbon nanotubes. *Phys Rev B* 2004;69:1154291–8.
- [181] Li C, Chou TW. A structural mechanics approach for the analysis of carbon nanotubes. *Int J Solids Struct* 2003;40:2487–99.
- [182] Wang CM, Zhang YY, Xiang Y, Reddy JN. Recent studies on buckling of carbon nanotubes. *Appl Mech Rev* 2010;63:1–18.
- [183] Chang T, Li G, Guo X. Elastic axial buckling of carbon nanotubes via a molecular mechanics model. *Carbon* 2005;43:287–94.
- [184] Hu N, Nunoya K, Pan D, Okabe T, Fukunaga H. Prediction of buckling characteristics of carbon nanotubes. *Int J Solids Struct* 2007;44:6535–50.
- [185] Kalamkarov AL, Georgiades AV, Rokkam SK, Veedu VP, Ghasemi-Nejhad MN. Analytical and numerical techniques to predict carbon nanotubes properties. *Int J Solids Struct* 2006;43:6832–54.
- [186] Ávila AF, Lacerda GSR. Molecular mechanics applied to single-walled carbon nanotubes. *Mater Res* 2008;11:325–33.
- [187] Nahas MN, Abd-Rabou M. Finite element modeling of carbon nanotubes. *Int J Mech Mech Eng* 2010;10:19–24.
- [188] To CWS. Bending and shear moduli of single-walled carbon nanotubes. *Finite Elem Anal Des* 2006;42:404–13.
- [189] Rahmandoust M, Öchsner A. On finite element modeling of single and multi-walled carbon nanotubes. *J Nanosci Nanotechnol* 2012;12:8129–36.
- [190] Yao X, Han Q, Xin H. Bending buckling behaviors of single- and multi-walled carbon nanotubes. *Comput Mater Sci* 2008;43:579–90.
- [191] Fan CW, Liu YY, Hwu C. Finite element simulation for estimating the mechanical properties of multi-walled carbon nanotubes. *Appl Phys A* 2009;95:819–31.
- [192] Rahmandoust M, Öchsner A. Buckling behaviour and natural frequency of zigzag and armchair single-walled carbon nanotubes. *J Nano Res* 2011;16:153–60.
- [193] Mir M, Hosseini A, Majzoobi GH. A numerical study of vibrational properties of single-walled carbon nanotubes. *Comput Mater Sci* 2008;43:540–8.
- [194] Che J, Cağın T, Goddard WA. Thermal conductivity of carbon nanotubes. *Nanotechnology* 2000;11:65–9.
- [195] Sammalkorpi M, Krasheninnikov A, Kuronen A, Nordlund K, Kaski K. Mechanical properties of carbon nanotubes with vacancies and related defects. *Phys Rev B* 2004;70:245416-1-8.
- [196] Georgantzinos SK, Giannopoulos GI, Anifantis NK. The effect of atom vacancy defect on the vibrational behavior of single-walled carbon nanotubes: a structural mechanics approach. *Adv Mech Eng* 2014;6:291645.
- [197] Garg A, Sinnott SB. Effect of chemical functionalization on the mechanical properties of carbon nanotubes. *Chem Phys Lett* 1998;295:273–8.
- [198] Xin H, Han Q, Yao XH. Buckling and axially compressive properties of perfect and defective single-walled carbon nanotubes. *Carbon* 2007;45:2486–95.
- [199] Amjadipour M, Dao DV, Motta N. Vibration analysis of initially curved single walled carbon nanotube with vacancy defect for ultrahigh frequency nanoresonators. *Microsyst Technol* 2015;22:1–6.
- [200] Imani Yengejeh S, Öchsner A. On the stiffness of carbon nanotubes with spiral distortion. *J Nano Res* 2014;29:85–92.
- [201] Imani Yengejeh S, Öchsner A. Influence of twisting and distortion on the mechanical properties of carbon nanotubes. *J Comput Theor Nanosci* 2015;12:443–8.

- [202] Imani Yengejeh S, Kazemi SA, Öchsner A. Influence of combined loading on the structural stability of carbon nanotubes. *Mater Chem Phys* 2015;158:96–106.
- [203] Imani Yengejeh S, Kazemi SA, Öchsner A. On the buckling behavior of curved carbon nanotubes. In: Öchsner A, Altenbach H, editors. *Mechanical and materials engineering of modern structure and component design*. Switzerland: Springer International Publishing; 2015. p. 401–12.
- [204] Imani Yengejeh S, Delgado JPQ, Barbosa de Lima AG, Öchsner A. Numerical simulation of the vibration behavior of curved carbon nanotubes. *Adv Mater Sci Eng* 2014;2014:1–9.
- [205] Imani Yengejeh S, Öchsner A. Influence of structural imperfections-twisting and distortion-on the vibrational behavior of carbon nanotubes, *Proceedings of the Institution of Mechanical Engineers. Part N: Journal of Nanomaterials, Nanoengineering and Nanosystems* 2016;230:2397–7922.
- [206] Lu Q, Bhattacharya B. Effect of randomly occurring Stone-Wales defects on mechanical properties of carbon nanotubes using atomistic simulation. *Nanotechnology* 2005;16:555–66.
- [207] Shariati AA, Golkarian AR, Jabbarzadeh M. Investigation of vibrational behavior of perfect and defective carbon nanotubes using non-linear massespring model. *J Solid Mech* 2014;6:255–64.
- [208] Imani Yengejeh S, Akbar Zadeh M, Öchsner A. On the tensile behavior of hetero-junction carbon nanotubes. *Composites Part B* 2015;75:274–80.
- [209] Imani Yengejeh S, Akbar Zadeh M, Öchsner A. Numerical characterization of the shear behavior of hetero-junction carbon nanotubes. *J Nano Res* 2014;26:143–51.
- [210] Imani Yengejeh S, Akbar Zadeh M, Öchsner A. Numerical modeling of eigenmodes and eigenfrequencies of hetero-junction carbon nanotubes with pentagon-heptagon pair defects. *Comput Mater Sci* 2014;92:76–83.
- [211] Imani Yengejeh S, Kazemi SA, Öchsner A. A numerical evaluation of the influence of atomic modification on the elastic and shear behavior of connected carbon nanotubes with parallel longitudinal axes. *J Nano Res* 2014;29:93–104.
- [212] Imani Yengejeh S, Kazemi SA, Öchsner A. On the influence of atomic modifications on the structural stability of carbon nanotube hybrids: numerical investigation. *Int J Appl Mech* 2014;6:1450077.
- [213] Qin Z, Qin QH, Feng XQ. Mechanical property of carbon nanotubes with intramolecular junctions: molecular dynamics simulations. *Phys Lett A* 2008;372:6661–6.
- [214] Liu WG, Meng FY, Shi SQ. A theoretical investigation of the mechanical stability of single-walled carbon nanotube 3-D junctions. *Carbon* 2010;48:1626–35.
- [215] Kang Z, Li M, Tang Q. Buckling behavior of carbon nanotube-based intramolecular junctions under compression: molecular dynamics simulation and finite element analysis,. *Comput Mater Sci* 2010;50:253–9.
- [216] Sarma JVN, Chowdhury R, Jayaganthan R, Scarpa F. Atomistic studies on tensile mechanics of BN nanotubes in the presence of defects. *Int J Nanosci* 2014;13:1–9.
- [217] Jiang L, Guo W. A molecular mechanics study on size-dependent elastic properties of single-walled boron nitride nanotubes. *J Mech Phys Solids* 2011;59:1204–13.
- [218] Rahmandoust M, Öchsner A. Influence of structural imperfections and doping on the mechanical properties of single-walled carbon nanotubes. *J Nano Res* 2009;6:185–96.
- [219] Ghavamian A, Öchsner A. A Comprehensive numerical investigation on the mechanical properties of hetero-junction carbon nanotubes. *Commun Theor Phys* 2015;64:215–30.